Insulator-based Dielectrophoresis for Bacterial Characterization and Trapping

Diana Nakidde

Thesis submitted to the faculty of the Virginia Polytechnic Institute and State University in partial fulfillment of the requirements for the degree of

Master of Science
in
Electrical Engineering

Masoud Agah, Chair
Kwang-Jin Koh
Chenming Zhang

February 27th 2015
Blacksburg, VA USA

Keywords: Microelectromechanical Systems (MEMS), Dielectrophoresis (DEP), Microfabrication, *Staphylococcus aureus* (*S. aureus*), Isulator-based Dielectrophoresis (iDEP)

Insulator-based Dielectrophoresis for Bacterial Characterization and Trapping

Diana Nakidde

Abstract

This work was focused on the characterization of microparticles with particular emphasis on waterborne pathogens which pose a great health risk to human lives. The goal of this study was to develop microfluidic systems for enhanced characterization and isolation of bioparticles. Insulator – based dielectrophoresis (iDEP) is a promising technique for analyzing, characterizing and isolation of microparticles based on their electrical properties. By employing insulator-based constrictions within the microchannel in combination with microelectrodes within the vicinity of the electrodes, dielectrophoretic performance is enhanced. In this study, three dimensional insulator-based dielectrophoresis devices are fabricated using our in-house developed 3D micromachining technique. This technology combines the benefits of electrode-based DEP, insulator-based DEP, and three dimensional insulating features with the goal of improving trapping efficiency of biological species at low applied signals and fostering wide frequency range operation of the microfluidic device. The dielectric properties of bacteria as well as submicron polystyrene beads are discussed and the impact of these results on the future development of iDEP microfluidic systems is explored.

This study was primarily funded by the National Science Foundation under award number ECCS - 1310090.

Acknowledgements

First, I would like to thank my advisor, Dr. Masoud Agah, for his invaluable guidance and support throughout this work. I have learned a great deal from him and grown immensely both as an individual and as a professional. I'm grateful for the opportunity he afforded me to learn from him and to work with a brilliant and resilient group of individuals.

I would like to thank current and former colleagues of the VT MEMS Lab. I would especially like to thank and acknowledge Dr. Phillip Zellner for his innovative technical contribution to this work. I'm equally indebted to Mrs. Vaishnavi Srinivasaraghavan for her boundless well of knowledge and her willingness to share it. Dr. Shree Narayanan, Mr. Hesam Babahosseini, Ms. Sarah El-Helw, Dr. Hamza Shakeel, Mr. Yahya Hosseini, Mr. Tyler Shake, Mr. Apoorva Garg, Ms. Deepti Aggarwal, and Ms. Huaning Zhao are all excellent engineers with bright futures ahead of them, their advice and guidance is much appreciated.

I would like to thank my family for the love and support. I'm immensely grateful for my mom, Rose Ssemuju, for believing in me and being a great role model. Her work ethic is an indispensable lesson I have learned. Special thanks to my dad Thomas More Ssemuju and my brothers Henry, Joseph, Paul and Michael. I'm heartily thankful for the selfless contributions of my sister, Liz N. Nangendo, this work would not have been possible without her.

Lastly, I give glory to my Lord and father!

Dedicated to My family, and to My Lord and Father

Contents

Figures

Tables

1.0 Introduction

1.1 Significance and Background

Water is a part of all forms of life, yet many lack access to clean water and are vulnerable to waterborne bacterial infections. The importance of characterizing and detecting pathogenic bacteria strains and emerging pathogens cannot be understated. While access to a treated water supply is the norm in the developed world, access to clean water and sanitation in the developing world are not the rule and therefore waterborne infections are rampant.

According to the World Health Organizations, almost 2.5 billion people lack access to an improved water supply and sanitation. It is estimated that 1.8 billion people use a source of drinking water that is feacally contaminated [1]. With 2 million annual deaths attributed to unsafe water, sanitation and hygiene, from these more than 50% are microbial intestinal infections.

Generally, ingesting water contaminated with human and animal waste is a great microbial infection risk. Wastewater discharges into coastal and fresh water systems introduce pathogens into the water system [2]. This holds true in the developed and developing world. In the USA, it's been estimated that 560,000 people suffer from severe waterborne diseases while 7.1 million suffer from some form of mild to moderate microbial infection leading to an estimated 12,000 deaths a year [3, 4].

Microelectromechanical systems is commonly represented by the acronym MEMS that was officially adopted by a group of 80 zealots at a Micro Tele-operated Robotics Workshop in Salt Lake City in 1989 [5]. Microelectromechanical systems refer to devices with a characteristic length of less than 1000µm but more than 1µm that combine mechanical and electrical components. Initially MEMS were fabricated using integrated circuit batch-processing technologies, but lately unique MEMS-specific micromachining processes are being developed. *Figure 1.1* shows some intricate MEMS devices fabricated using MEMS technology. This multidisciplinary technology is exponentially progressing at a rate that exceeds our understanding of the physics involved. Some of the MEMS devices that have been fabricated include actuators, motors, valves, gears,

cantilevers, diaphragms, microfluidic channels and tweezers. These have then been applied in systems as sensors for pressure, temperature, mass flow, velocity, sound, and biological analysis.

The miniaturization of nearly all device systems is arguably one of the greatest opportunities for commercial profit and technological advancement. This is especially true for micromechanical, microfluidic, microthermal, micromagnetic, microoptical and micromechanical systems [6]. A microfluidic system is a MEMS technology that manipulates small volumes of fluids using channels with dimensions of 10-1000μm [7].

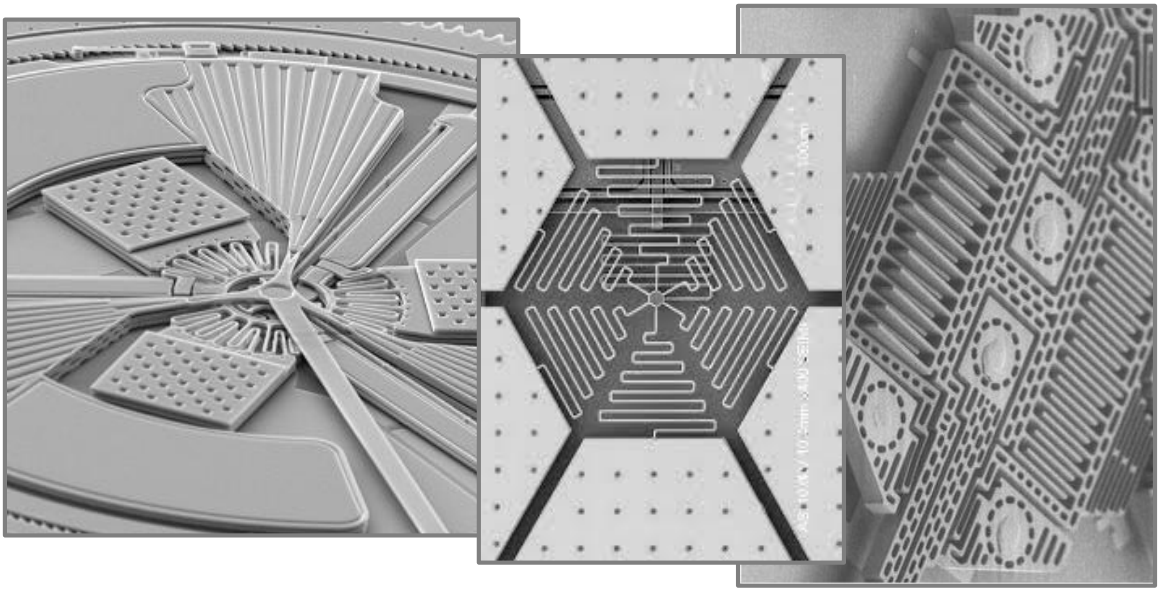

Figure 1.1: Intricate MEMS devices fabricated using MEMS technology. *MEMSnet - www.memsnet.org, Bacteria World - www.bacteria-world.com, AGS Tech - www.agstech.net, and MEMX - www.memx.com.* Used under fair use, 2015.

1.2 Theory

Dielectrophoresis (DEP) is a term that was first adopted by Pohl [8]. It originates from the Greek word *phorein* that describes the effect of a particle being carried as a result of its dielectric properties. Dielectrophoresis and electrophoresis are closely related phenomena that describe the movement of particles under the effect of an applied field. Whereas electrophoresis is the movement of charged particles in direct current (DC) or low frequency alternating current (AC) fields, dielectrophoresis is the motion of

suspended particles relative to the surrounding medium due to polarizing forces generated in a non-uniform electric field. Particles are generally <1000 µm in range and this is mostly because gravity effects prevail in larger particles.

An applied electric field will induce dipole charges within the material of polarizable particle. For a uniform field, the forces on the dipole charges are equal and opposite and therefore create a net zero force. In a non-uniform electric field, on the other hand, opposing forces on the dipole are unequal resulting in a net force on the particle. Therefore, depending on the relative polarity of the particle with respect to the surrounding medium, it is induced to move to the high electric field region (positive DEP - pDEP) or towards the weaker field region (negative DEP - nDEP) as shown in *Figure 1.2*.

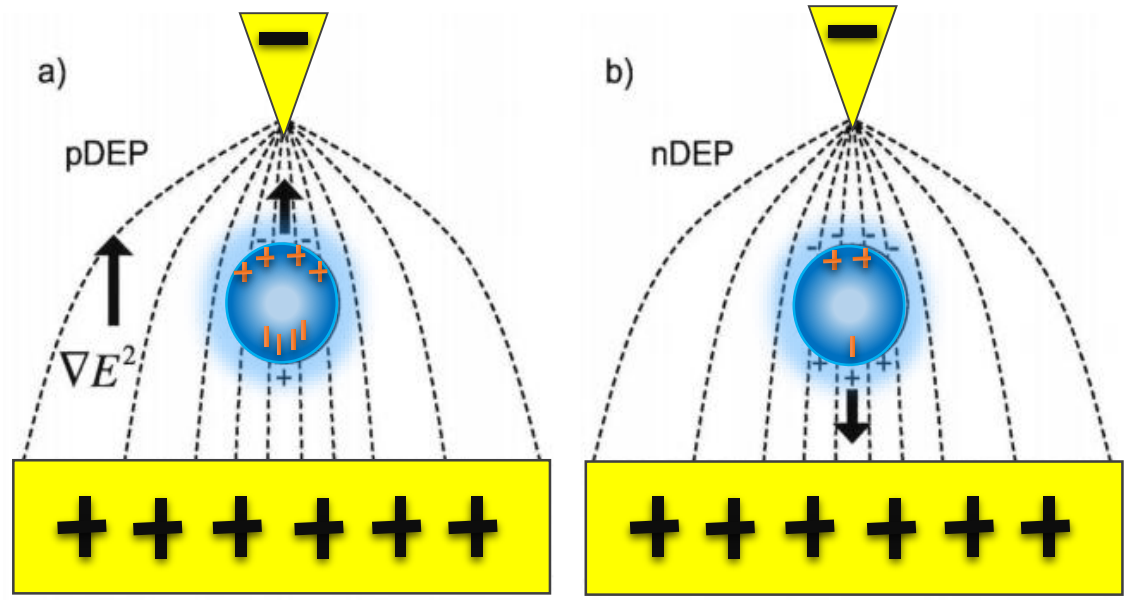

Figure 1.2. a) Particle experiencing positive DEP is drawn to the strongest electric field. b) Particle experiencing negative DEP is drawn to the weaker field region

Following established theory where E is the applied electric field, the DEP force $\mathbf{F_{DEP}}$ felt by spherical particle of radius R suspended in a medium of dielectric permittivity ε_m is given by:

$$\mathbf{F_{DEP}} = 2\pi R^3 \varepsilon_m Re\left[f_{CM} \right] \nabla(\mathbf{E} \bullet \mathbf{E}) \qquad (1)$$

Re [f_{CM}] is the real part of the Clausius-Massoti (CM) factor which is:

$$f_{CM} = \left(\varepsilon_p^* - \varepsilon_m^*\right) / \left(\varepsilon_p^* + 2\varepsilon_m^*\right) \qquad (2)$$

where ε_p * and ε_m * are the complex permittivities of the particle and the medium, respectively. Complex permittivity is defined as:

$$\varepsilon^* = \varepsilon + \sigma / (j\omega) \qquad (3)$$

ε and σ are the real permittivity and conductivity while ω is the angular frequency of the applied electric field.

Notably, at DC or low frequency AC fields, the DEP separation capability is dominated by the particle size due to the cubed radius term in Equation 1. Alternatively, at high frequencies, the DEP separation is mostly influenced by the CM factor because the high fields are capable of penetrating the cell membrane into the electrically distinct cytoplasm. The crossover frequency, at which DEP force crosses from nDEP to pDEP or vice versa, is used to separate different sample populations.

2.0 THREE DIMENSIONAL PASSIVATED-ELECTRODE INSULATOR-BASED DIELECTROPHORESIS (3D ııDEP)

Acknowledgement

This work was initiated by Dr. Phillip Zellner during his PhD research. I acknowledge his innovative technical contribution to this study. I also acknowledge the contributions of Mohammad Mehdi Alemi, Tyler Shake, Yahya Hosseini, Maria Riquelme, Dr. Amy Pruden and Dr. Masoud Agah who are co-authors on this manuscript. This manuscript was recently accepted for publication in Biomicrofluidics Journal [9]. dx.doi.org/10.1063/1.4913497

2.1 Introduction

Dielectrophoresis is a well-known technique for moving, separating and trapping micron scale particles [10]. It is particularly useful for manipulating biological samples which usually fall within the micron size range. One of its greatest strengths is the ability to manipulate several independent variables like signal magnitude, applied frequency, signal combinations, electrode spacing and microstructure orientation to achieve highly selective trapping. This technique has been widely used in biological applications to characterize yeast [11], bacteria [12] and mammalian cells [13].

Electrode based DEP (eDEP) technique is normally used to generate non-uniform electric fields in the channel [14]. Micro-patterned electrodes in the channel generate highly localized electric fields and trapping is observed to be concentrated around the electrodes. Insulator based DEP (iDEP), on the other hand, uses insulating structures rather than embedded electrodes to generate non-uniform electric field gradients in the microchannel. iDEP devices have been employed in the past to characterize particles including bacteria, viruses, cells, and beads [15-17].

Previously, three dimensional insulator-based dielectrophoresis (3D iDEP) devices have been used to increase sensitivity of iDEP devices. Use of 3D insulating features has been

shown to increase electric field gradient and the DEP force acting on particles. Previous studies using 3D iDEP technology have been shown to effectively trap bacteria [18]. Earlier work by our group focused on trapping and separation of particles using silicon DC-Biased iDEP devices [19]. Furthermore, because silicon microfluidic devices were investigated in comparison to polymer devices, this study demonstrated greatly improved heat dissipation effects attributed to enhanced thermal dissipation properties of silicon over polymer substrates.

In this paper, a DEP technique that exploits the benefits of iDEP, eDEP and 3D fabricated insulating microstructures is demonstrated. A three dimensional, passivated-electrode, insulator-based dielectrophoresis device (3D πDEP) is introduced for the first time. A schematic of the 3D πDEP device is shown in *Figure 2.1*. The electrodes are fabricated separately on a glass slide; they can be embedded in the channel, or capacitively coupled through a thin 100µm glass slide and reused over multiple runs. In this study, the electrodes were passivated through a thin 100um glass slide and this offers a lot of flexibility in the design of the electrodes so as to achieve optimal electric fields across the microfluidic channel. In previous work, a three dimensional insulator-based device has been shown to demonstrate enhanced performance using a combination of DC coupled AC signals [20].

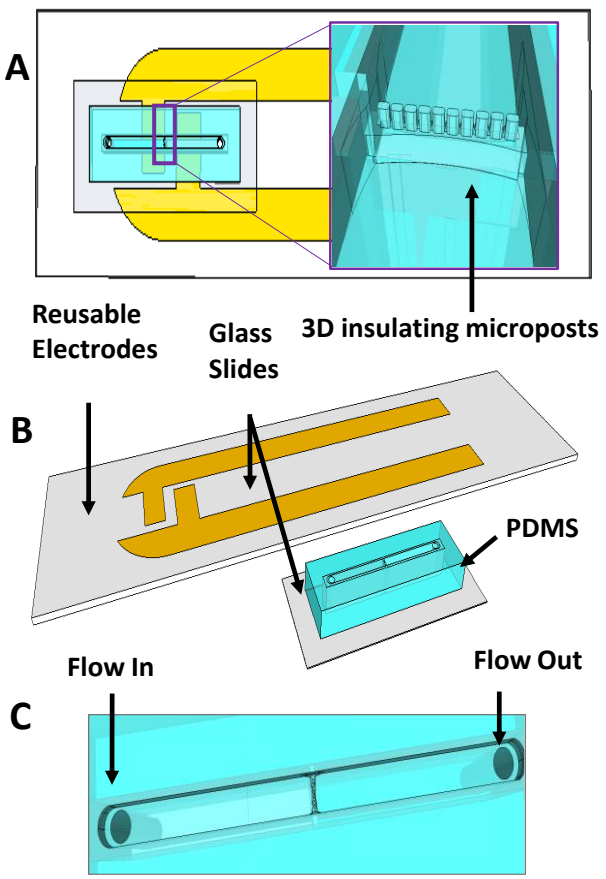

Figure 2.1: Schematic of 3D πDEP. **A.** Top view showing reusable electrodes, microfluidic device and 3D insulating features. **B.** Isometric view showing material composition. **C.** Front view showing the main channel.

In this previous work demonstrated by our group, the electrodes were in contact with the medium. This caused the electrodes to be located farther away from the insulating microstructures responsible for generating electric field gradient. In these iDEP devices, the voltages are applied across a significant portion of the microchannel increasing the complexities due to heating effects [21, 22]. In the current study, electrodes are located within the vicinity of the insulating microposts to minimize heat build-up within the channel. Reduced electrode spacing minimizes the conductive path travelled by the current ultimately reducing heat generated within the microchannel. The DEP force is achieved by 3D insulating structures in the channel. In comparison to traditional iDEP devices with 2D insulating features, 3D features increase the electric field gradient which in turn increases the DEP force. 100% trapping efficiency can be achieved at low applied voltages thus reducing power consumption, the adverse effects of electrothermal flow and allowing for integration with simpler supporting electronics.

This 3D πDEP is comparable to our previously reported passivated-electrode insulator-based dielectrophoresis (OπDEP) device [23]. OπDEP combines the benefits of a high throughput, low cost 2D iDEP and the enhanced sensitivity of eDEP with electrodes located in the vicinity of the 2D insulating microstructures. A reusable set of electrodes are activated and the signal capacitively coupled through a thin glass slide into the microfluidic channel. 3D πDEP, on the other hand, achieves high capture efficiencies at lower applied voltages and over a wider frequency range. This paper will demonstrate performance of the 3D πDEP microfluidic device by trapping live and dead *Staphylococcus aureus* bacterial cells. Enrichment and separation of this bacterial cell is especially important because *S. aureus* is an ubiquitous opportunistic pathogen, whose infections are becoming increasingly difficult to treat due to the emergence of multiple-antibiotic resistant strains in recent years.

2.2 Theory

The motion of polarizable particles suspended in a dielectrically dissimilar media when subjected to a spatially non-uniform electric field is dielectrophoresis (DEP) [24]. Unlike electrophoresis, particles do not have to possess a net charge to be polarized by DEP

forces and hence, non-conducting particles can be manipulated by DEP. The DEP force acting on a spherical particle suspended in an electrolyte is [25]:

$$F_{DEP} = 2\pi R^3 \varepsilon_m \,\mathrm{Re}\left[f_{CM} \right] \nabla \left(E \bullet E \right) \quad (2.1)$$

where R is the radius of the particle, ε_m is the permittivity of the medium, **E** is the local electric field. R_e [f_{CM}] is the real part of the Clausius - Mossotti (CM) factor which is [25]:

$$f_{CM} = \frac{\left(\varepsilon_p{}^* - \varepsilon_m{}^* \right)}{\left(\varepsilon_p{}^* + 2\varepsilon_m{}^* \right)} \quad (2.2)$$

where ε_p^* and ε_m^* are the complex permittivities of the particle and the medium, respectively. Complex permittivity is defined as [25]:

$$\varepsilon^* = \varepsilon + \frac{\sigma}{j\omega} \quad (2.3)$$

Because of the complex permittivity, $\mathbf{F}_{DEP}$ is a function of frequency and can take on positive or negative values depending on the CM factor equation (2.2). The polarity of the DEP force, $\mathbf{F}_{DEP}$ will therefore depend on the applied signal frequency. To further understand the behaviour of biological particles under electric fields, a shell model is employed, describing a cell as a sphere of highly conductive cytoplasm encased in insulating membrane [26]. At DC fields and low frequencies (f < 500 Hz), the DEP force is governed by particle size and conductivity. At high frequencies (f > 500 Hz), the complex nature of the cell significantly contributes to the DEP response. For cells with effective permittivity greater than the conductivity of the surrounding medium, a positive CM factor and thus a positive DEP force (pDEP) is experienced. Negative DEP force is experienced otherwise. A crossover frequency is determined when zero DEP force acts on the particle and it occurs when the changing DEP force transitions from pDEP to nDEP and vice versa. Since the DEP force near a crossover frequency is close to zero (it is zero when $f_{cm} = 0$), this allows for particle separation using the DEP technique.

Pressure driven fluid, at a low Reynold's number, moves through the microfluidic channel and imposes a drag force on a spherical particle. This drag force is given by [10]:

$$F_{Drag} = 6\eta R\pi\left(u_{pf}\right) \quad (2.4)$$

where R is the radius of the particle, η is the dynamic viscosity of the fluid, and u_{pf} is the relative velocity of the particle with respect to the fluid. To trap a particle in a DEP device, the acting DEP force must be equal to or greater than the drag force ($\boldsymbol{F}_{DEP} \geq \boldsymbol{F}_{Drag}$). As shown in equation 2.4, an increase in the flow rate of the medium necessitates a higher DEP force to trap the particles.

Electrical field signals are applied to the 3D πDEP device by capacitively coupling through a thin glass slide in contact with the electrode substrate into the microfluidic channel. 3D insulating (PDMS) microstructures in the centre of the microchannel create constrictions dividing the two halves of the channel as shown in *Figure 2.1*. These PDMS microstructures have a higher impedance in comparison with the media flowing through them such that when an electric field is applied to the microfluidic device, current takes the path of least resistance – 36 μm wide and 22 μm deep openings through the 3D microstructure constrictions. Because the bulk of the current is compressed through these constrictions, high electric field gradients are generated at the microposts: this is the main operating principle of iDEP devices and subsequently πDEP devices. The generated electric field gradients, which directly influence DEP force experienced in the channel, are dependent on the geometry and physical dimension gradient of the insulating structures. The ability to vary structures in three dimensions allows for constriction of electric fields and current in all dimensions thereby creating high geometric gradients. We have shown in the past that DC iDEP devices with 3D gradients generate stronger DEP forces in comparison to 2D gradient iDEP devices [19]. Similarly, the new 3D πDEP devices can operate at lower applied voltages which ultimately decreases joule heating complications that usually plague iDEP devices [27]. Additionally this limits electrothermal flow, which is a parasitic effect that creates complications in iDEP devices [28].

2.3 Methods and Materials

A. Numerical Device Modeling

A numerical model of the 3D πDEP devices is created using COMSOL Multiphysics 3.5 (COMSOL Inc., Burlington, MA) under the AC/DC module so as to explore electric field distributions within the microchannel. A 3D COMSOL model is created for the device under investigation. The electrical conductivities used for PDMS, glass, air, and deionized water (DI) are 8.20×10^{-13} S/m, 1.25×10^{-9} S/m, 3.00×10^{-9} S/m, and 8.00×10^{-4} S/m, respectively. The electrical permittivities used for PDMS, glass, air, and deionized water are 2.65, 4.65, 1, and 80, respectively. To define boundary conditions, the electrodes are assigned AC electric potentials while all other boundaries are defined as electrical insulation. The values for PDMS were set by the manufacturer. The numerical modelling and simulations are used to evaluate the values of $\nabla|\mathbf{E}|^2$ as a function of position in the microchannel and applied frequency signal. This model affirms the concept in equation 4.1, showing that the DEP force experienced by a given particle in medium is proportional to $\nabla|\mathbf{E}|^2$.

B. Device Fabrication

A new process flow for the design and fabrication of the 3D πDEP is implemented in PDMS as shown in *Figure 2.2*. Initially a layer of thermal silicon dioxide, 0.4μm thick, is grown at 1000 °C on a <100> silicon wafer. The oxide layer is used as a mask during the etch process. Using our 3D silicon micromachining technique [29-31], a photomask layout consisting of an array of rectangular openings with different sizes and aspect ratios is created (*Figure 2.2A*). Thereafter photoresist (S1813) is patterned and the pattern is transferred to the oxide using an Alcatel AMS-100 Deep Reactive Ion Etcher (DRIE) with CH_4 plasma. The DRIE etch exposes silicon, which is isotropically etched using SF6 plasma (*Figure 2.2B*). The reactive ion etch lag (RIE lag) and its dependency on the geometrical patterns of the mask layout is exploited to create 3D cavities and microposts. This technique provides three dimensional flexibility over structure formation. Next, photoresist is removed and the silicon substrate is bonded to a Pyrex wafer under vacuum

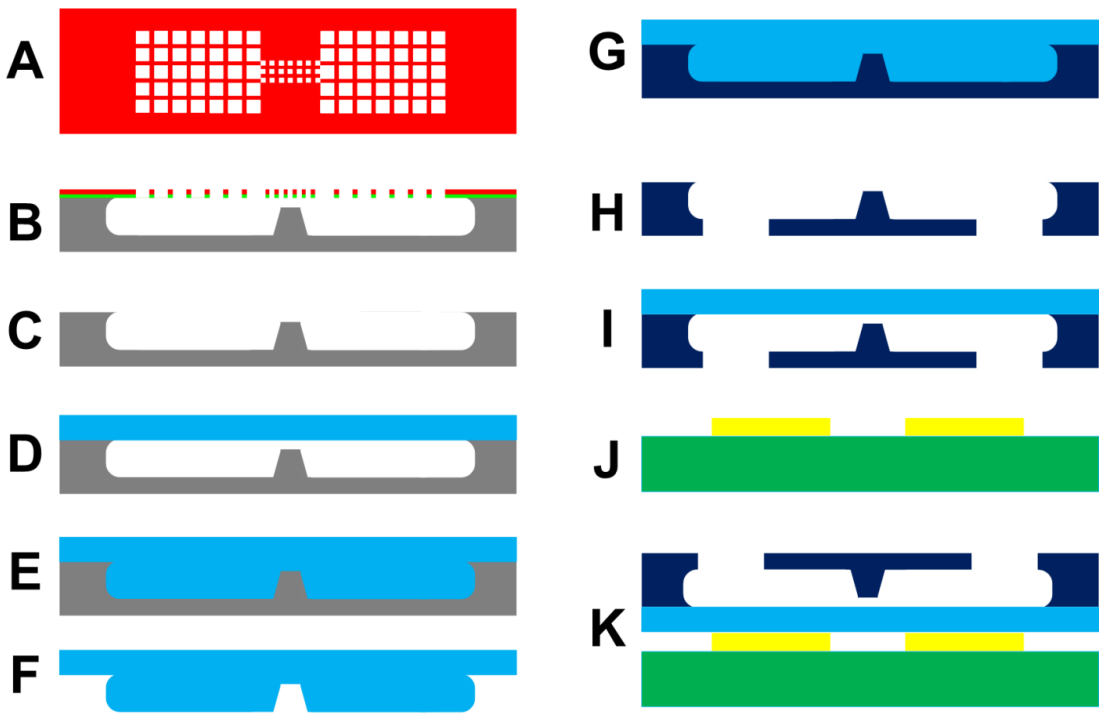

Figure 2.1: 3D πDEP device fabrication process flow. **A.** Top view of DRIE lag mask design. **B**. Pattern oxide mask and then use RIE lag 3D silicon etch. **C**. Remove oxide lattice structure with BOE. **D**. Anodically bond silicon to Pyrex wafer under vacuum. **E.** Melt Pyrex into silicon mold. **F.** Etch all silicon with KOH. **G.** Pour PDMS over Pyrex master and cure. **H.** Remove PDMS from glass master and punch ports. **I.** Plasma bond to glass slide. **J.** Evaporate electrodes on separate glass substrate. **K.** Align electrodes and microfluidic device prior to experimental runs

(Figure 2.2C and 2.2D). The Pyrex wafer is melted at high temperatures under a furnace causing the molten glass to conform to the shape of the 3D silicon features (*Figure 2.2E*) [30]. The glass substrate master mold is left behind after the silicon substrate is etched away using KOH (*Figure 2.2F*). Low cost PDMS devices were mass produced using the glass master mold. Liquid PDMS (Sylgand 184 Silicon elastomer kit, Dow Corning, Midland, MI) was mixed in a 10:1 ratio of PDMS monomer and curing agent, and poured onto the glass mold (*Figure 2.2G*). The setup was put into a vacuum chamber for 1 hour to remove gas bubbles and then cured for 8 hours at 90 ºC to create 3D PDMS microstructures. Subsequently, the multiple device PDMS polymer was carefully peeled off the mold, cut into single devices, and 2 mm holes were punched into microfluidic channels for fluidic ports (*Figure 2.2H*). The devices are sealed by plasma bonding using a Plasma Cleaner (Harrick Plasma) to a size #0 glass cover-slide (Electron Microscopy Sciences) (*Figure 2.2K*), which is 100 µm thick, forming the microfluidic cartridge.

Notably, microfluidic devices of different designs can be created on a single wafer and fabricated at the same time. Additionally, many PDMS devices can be created from the same glass master mold, saving more resources.

Electrodes were made on a separate Pyrex glass substrate using lift off technique. Photoresist (AZ9260, AZ Electronic Materials) was used to pattern the glass substrate. Thereafter, a thin layer (25 nm) of chrome and a thicker layer (200 nm) of gold were deposited using e-beam evaporation (PVD-250, Kurt J. Lesker Company). The excess metal was later removed by dissolving the photoresist in acetone (*Figure 2.2J*). The fabricated electrodes were 4 mm long, 6mm wide and 1.2 mm apart. Under experimental runs, the PDMS microfluidic chip is placed on top of the electrodes glass substrate with the 3D insulating structures aligned between the electrodes spacing (*Figure 2.2K*). In this configuration, the electrodes span across the entire width of the channel allowing for uniform distribution of electric fields across the 3D insulating microstructures. Over multiple experimental runs, the PDMS microfluidic device can be replaced to maintain sample purity while the electrodes are reused. Alternatively, the electrodes can be embedded within the channel to increase device sensitivity. The two device components of the 3D πDEP device are shown in *Figure 2.3*.

Scanning electron microscopy (SEM) images, showing structural details of the 2 cm long microfluidic channel are shown in *Figure 2.4*. The main fluidic channel has a cross-section of 2.2 mm wide and 100 µm deep with 3D insulating microstructure obstacle, which splits up into 14 smaller channels, at the centre of the channel. The cross section of these smaller channels is 36 µm wide and 22 µm deep. Notably, the fabricated features have

Figure 2.3: Optical image of 3D πDEP device. (Top) Disposable microfluidic cartridge. (Bottom) Reusable gold electrodes

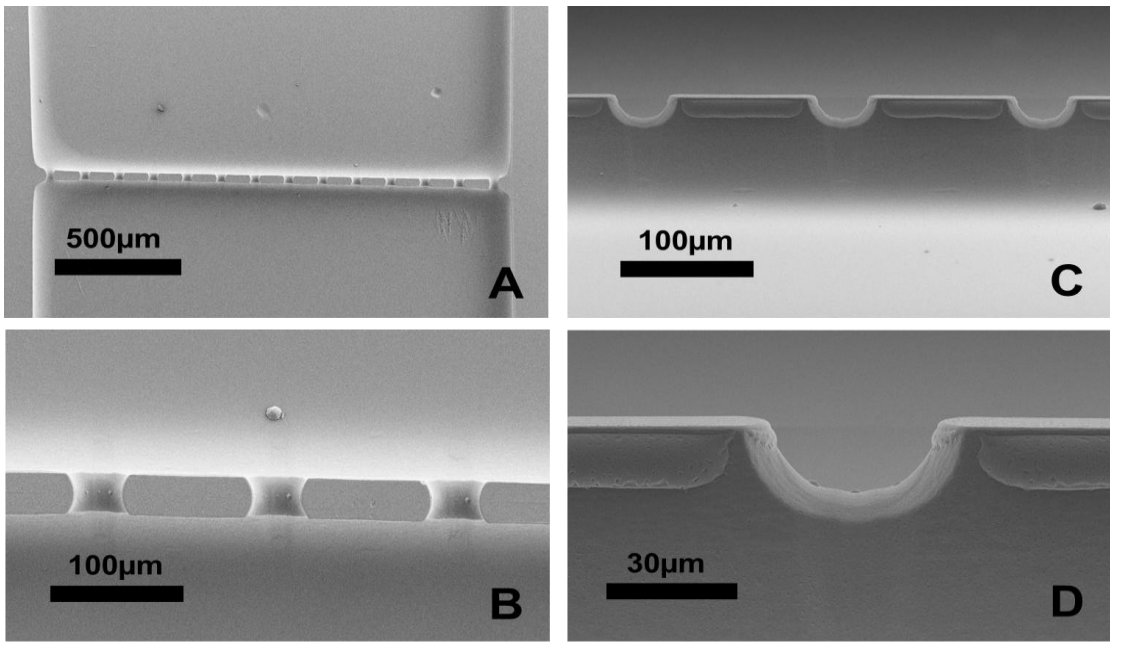

Figure 2.4: SEM of a πDEP device comprised of 3D microposts. **A.** Top view of device. **B.** Magnified top view showing 3D posts. **C.** Cross section of the posts showing the depth change of the structures. **D.** Magnified cross section showing constriction

rounded corners acquired by silicon isotropic etching: this is in contrast to sharp edges typically found in conventional microchannels. Therefore, the 3D aspect accounts for abrupt changes in cross-sectional area without the limitation of sharp edges.

C. Cell Preparation

Staphylococcus aureus (*S. aureus*) strain (ATCC 12600) was cultured in brain heart infusion media (Bactrius Limited, Houston TX). *S. aureus* cells were cultured in 100 ml of broth medium at 37 °C and 165 rpm to the exponential growth phase (OD600 ~ 0.8). Cells were then transferred into two sterile 50 ml centrifuge tubes, and subjected to five washes by centrifugation (5000 × g for 10 min) and re-suspension in 1× PBS. A calibration curve relating OD600 to microscopic cell counts was created and used to quantify the washed bacteria via spectrophotometry thereafter. To express green or red fluorescence under a microscope, bacteria were stained for 20 minutes using a Live/Dead viability kit (LIVE/DEAD Backlit, Invitrogen). Prior to experimental runs, *S. aureus* cells were centrifuged and re-suspended 5 times in deionized water with a measured conductivity of 800 µS/m. The deionized water conductivity was measured with a

solution conductivity meter (SG7, Mettler Toledo, Scherzenbach, Switzerland). The average cell concentration for experiments was 10^9 cells/ml.

D. Experimental Setup

An AC signal of 200V peak to peak (Vpp) was applied to the microfluidic device over a frequency range of DC to 1MHz using a function generator (4079, BK Precision) connected to a power amplifier (Voltage Amplifier A800DI, FLC Electronics). The PDMS-based microfluidic cartridges were placed in vacuum for at least 30 minutes prior to experiments to counter priming issues, remove contaminants, and eliminate air bubbles in the main channel. During experimental runs, the medium was pressure driven through the 3D πDEP device, using a 1 ml syringe connected to syringe pump (Pump 11 Elite, Harvard Apparatus), to a waste reservoir. Once the device was ready for operation, medium was continually pushed through the main channel at 100 µl/hr for 5 minutes prior to the beginning of the experiments in order to ensure steady fluid flow during operation. Because of the transparent PDMS-based microfluidic cartridge, DEP trapping efficiency of the device was observed in real time using an inverted fluorescent microscope (Axio Observer Z1) and video recording of all trapping experiments acquired using either CCD colour camera (AxioCam MRC) or a CCD monochrome camera (IDT Limited, MotionXtra NX-4) for high frame rate capture.

While maintaining a constant flow rate, for every experimental data point, a known electric signal was applied and the corresponding real time video recorded in real time. The signal was switched off after 40 seconds and previously trapped bacteria were released. Whenever necessary, the microchannel was cleared of fouled bacteria by increasing the flow rate of the medium. Thus, each data point accounted for bacteria trapped during that experimental run.

In order to quantify the effectiveness of the DEP trapping during experiments, light intensity measurements were conducted using Image J, an image analysis program developed by NIH. Two regions located at the microposts were selected and the intensity of fluorescent cells measured. This was quantified and compared to a region with no trapping to obtain the reported trapping efficiency (TE) defined as:

$$TE = \left[\frac{I - O}{I} \right] \times 100\% \quad (5)$$

where (I) is the trapping intensity of incoming bacteria and (O) is the trapping intensity of outgoing or escaped bacteria observed in the video during trapping. These measurements were made using Image J to quantify bacteria flow upstream (I) and downstream (O) of the 3D insulating microstructures trapping region. Notably, using this software, number of individual particles trapped can be counted by analyzing the area of fluorescent trapped regions for low concentration samples or larger bioparticles such as mammalian cells. Ultimately, the trapping efficiency from intensity measurements is undervalued since particles vertically pile up on the microposts when they are trapped.

Three fluid flow velocity sweeps from 100 μl/hr to 1000 μl/hr were conducted to observe influence of fluid flow on DEP trapping. The final reported data point representing one flow rate corresponds to values of I and O averaged over three flow sweeps. In situations where bacteria remained in clusters, the clusters were assumed to be flat and the size of the cluster was used to estimate the number of bacteria in the cluster. It should be noted that if clusters had multiple bacteria stacked in depth, then this method would underestimate the number of bacteria.

2.4 Results and Discussion

A. Numerical Modeling

The findings from numerical modelling are shown in Figure 15. $\nabla(\mathbf{E} \bullet \mathbf{E})$ was computed for an applied signal of 400 Vpp at 300 kHz. The top view and cross-section view of the slice plot of $\nabla(\mathbf{E} \bullet \mathbf{E})$ are shown in *Figure 2.5A* and *Figure 2.5B*, respectively. A PDMS structure molded the shape of the microfluidic channel. The analysis accounted for the DI water medium filling the entire channel. A thin glass slide passivation layer separated the medium from the activation layer of electrodes. Lastly, metal electrodes beneath the passivation layer were used to activate the device model. The electrical properties of the layers considered are shown in Table 1.

The frequency dependent model was activated using an applied electrical signal and then a parametric sweep was conducted over a range of frequencies from 10 Hz – 1 MHz to test the device model. The peak gradient was found to be 5.28×10^{17} $[(\mathrm{m\,kg^2})/(\mathrm{s^6A^2})]$. This is two orders of magnitude greater than the peak gradients using the exact same input signal in our previous iDEP devices [23] which only varied in two dimensions. To obtain an estimation of the Clausius-Massotti factor (f_{CM}), the electrical parameters of *S. aureus* bacteria and the surrounding DI water medium shown in Table 1 were used [17]. Using equations (2) and (3), real and imaginary values of f_{CM} were estimated using Matlab R2014a as shown in Figure 5D. Notably, the complex nature of

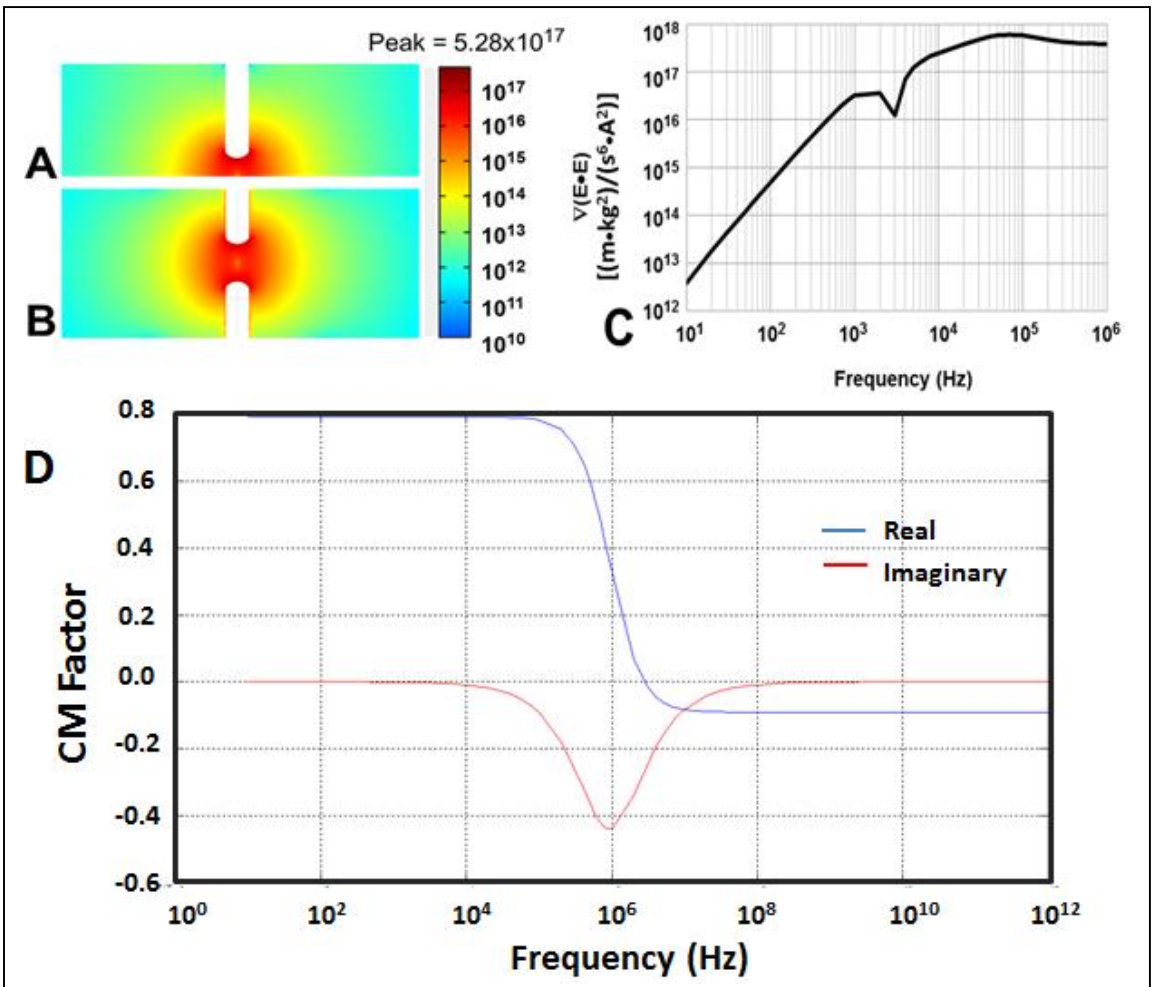

Figure 2.5: COMSOL simulations of electric fields in 3D πDEP devices. **A.** Side view of ∇(E•E) profile at 400 Vpp and 300 kHz. **B.** Top view of ∇(E•E) profile at 400 Vpp and 300 kHz. **C.** Maximum values of ∇(E•E) as a function of frequency. **D.** Simulated values of the real and imaginary Clausius-Massotti factor

bacteria cells, the unique oval shape, and the single shell model would further influence f_{CM}. The generated DEP force experienced by a bacteria in the 3D πDEP is a function of the simulated results of $\nabla(\mathbf{E} \cdot \mathbf{E})$ and f_{CM}.

As shown in equation 2.1, the DEP force acting on a particle is directly proportional to $\nabla(\mathbf{E} \cdot \mathbf{E})$. Therefore, because of the higher $\nabla(\mathbf{E} \cdot \mathbf{E})$ component, a much larger DEP force is generated by 3D πDEP devices for the same applied signal in comparison to 2D iDEP devices. Additionally, it is vital to note that electric field gradients in 3D πDEP devices vary in all three dimensions unlike gradients in 2D πDEP devices that only vary in two dimensions. The higher electric field gradients in 3D πDEP devices further account for stronger DEP forces experienced by particles.

The frequency response of the 3D πDEP device is shown in *Figure 2.5C*. Because the applied signal is capacitively coupled through a thin 100 µm glass slide that seals the microfluidic cartridge, the frequency response is analogous to a high pass filter with the attenuation increasing as the frequency is lowered. A dip in $\nabla(\mathbf{E} \cdot \mathbf{E})$ is observed at 2 kHz and this is attributed to the device operating near the resonant frequency of the circuit. There are several impedances both in series and in parallel to the active area of the device for which $\nabla(\mathbf{E} \cdot \mathbf{E})$ is calculated. This phenomenon is especially enhanced in capacitively coupled systems. Notably, the magnitude of the electric field gradient does not dip below

Material	Electrical Properties	
DI Water	Relative Permittivity, ε_m	80
	Electrical Conductivity, σ_m	0.0008 S/m
Glass	Density	965 kg/m^3
	Electrical Conductivity, σ	1.25 X 10^{-9} S/m
Metal Electrodes	Reference Resistivity, ρ	1.72 X 10^{-8} Ωm
	Electrical Conductivity, σ	5.998 X 10^7 S/m
S. aureus	Relative Permittivity, ε_p	60
	Electrical Conductivity, σ_p	0.01 S/m

Table 1: Electrical properties of material layers used in the modeling analysis

10^{15} $[(\mathrm{m\ kg^2})/\ (\mathrm{s^6A^2})]$ until the frequency is ~150 Hz. This model therefore predicts the ability of 3D πDEP devices to operate over a wide frequency range, including very low frequencies.

B. Frequency Response

DEP trapping experiments with *S. aureus* were conducted and a signal amplitude of 200 Vpp was maintained at an applied flow rate of 100 µl/hr. The experimental performance of the 3D πDEP device as a function of the applied frequency is shown in *Figure 2.6*. Under these conditions, DEP trapping with 80–100% capture efficiency was observed over a wide range of frequencies, from 600 Hz to 400 kHz for *S. aureus*. The reported results further support predictions from the numerical model. Because the strong DEP forces generated by the 3D πDEP are greater than $10^{15}[(\mathrm{m\ kg^2})/(\mathrm{s^6A^2})]$ over a broad frequency range, the microfluidic system is highly likely to achieve trapping over a wide frequency range. However, due to the limited bandwidth of the power amplifier used in our experiments, a decrease in capture efficiency is observed at higher frequencies.

The results showed that even at the lowest frequency tested (50 Hz), some bacteria were successfully trapped. At lower frequencies (20-100 kHz), it was observed that trapped bacteria tended to form extra elongated chains as shown in *Figures 2.6* and 2.*7*. This behaviour of bioparticles forming pearl chains when trapped in DEP devices has been previously reported [32]. At high frequencies (<200 kHz), however, trapping of bacteria was concentrated at the microposts with shorter pearl chains. This is attributed to stronger pDEP forces at high frequencies than at low frequencies, and these therefore pull the entire pearl chain to the 3D insulating microposts where the electric field gradient is greatest. A recorded video showing elongated chains of trapped bacteria at a low applied frequency of 100 kHz, and the bacteria being pulled in, constricted, and compacted at the microposts when the applied frequency is increased from 100 kHz to 300 kHz is shown (See Appendix 1 for the video) [19]. When the applied voltage signal was turned off, all previously trapped bacteria were released, thus trapping was found to be reversible.

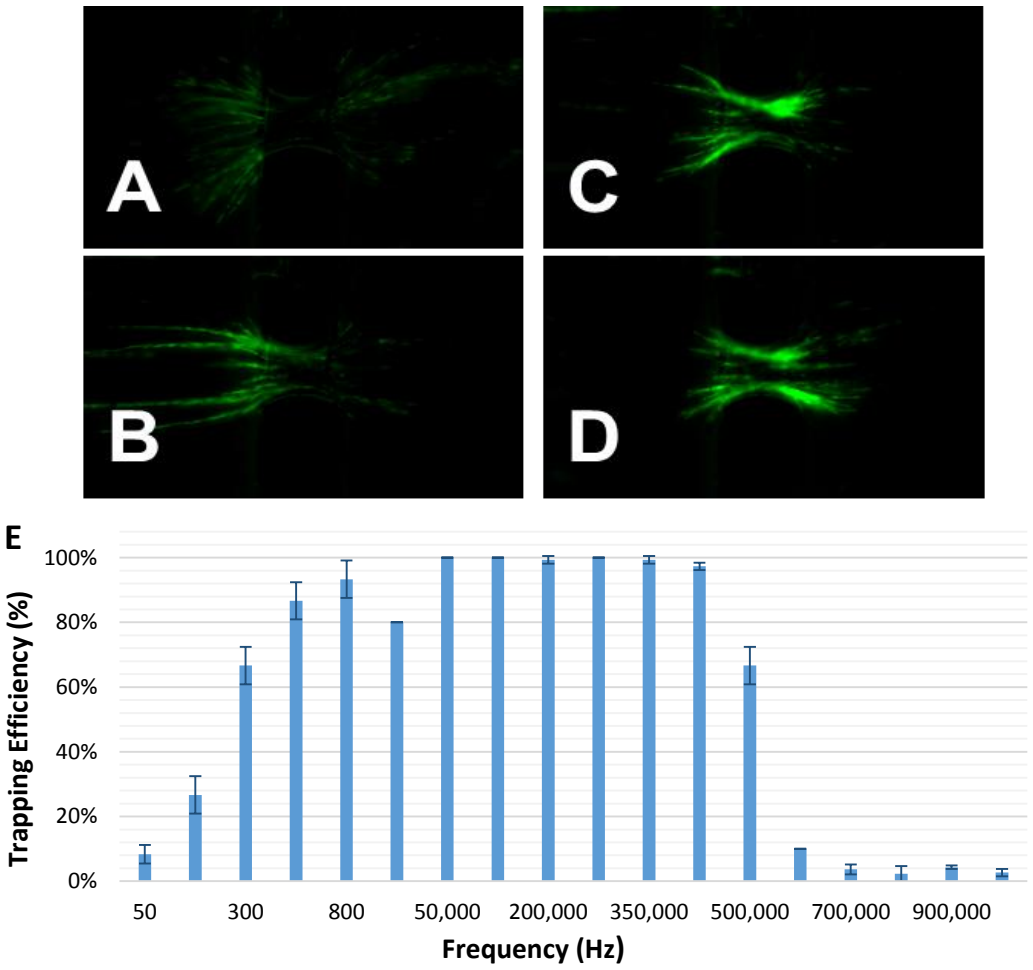

Figure 2.6: Images are of live *S. aureus* trapping **A.** 300Hz signal **B.** 3kHz signal b 30kHz signal **D.** 300kHz **E.** Trapping as a function of frequency (n=3).

C. Low Voltage Operation

With the frequency held constant, voltage sweeps were conducted over an experimentally determined device bandwidth. The flow rate was held constant at 100 µl/hr while the applied signal amplitude was gradually incremented from 0 - 450 Vpp. Variations in trapping efficiency with changing amplitude were recorded and the results are shown in *Figure 2.7*. Results showed that minimum trapping voltage rapidly decreased with increasing frequency. At 300 kHz, we observed trapping over 80% at voltages as low as 100 Vpp and the trapping gradually increased with increasing applied voltage. At 10 kHz, very low trapping efficiencies were recorded at applied signals below 300 Vpp.

Notably, we observed some trapping at the lowest applied voltage of 50 Vpp for all frequencies investigated as show in *Figure 2.7*. These results support the theory that at higher frequencies the particles experience stronger DEP force. Furthermore, this study demonstrates the capability to operate at lower applied voltages. The reported applied signals in 3D πDEP devices are significantly low compared to traditional iDEP device which typically require high voltages (~1000 Vpp) to operate [15, 16]. However, for iDEP devices utilizing 3D constrictions, lower operating voltages have been reported by researchers. Braff *et al.* reported some trapping of bacteria strains using a traditional iDEP device with 3D microstructures and electrodes in direct contact with the solution [18, 33]. In our previous work with 3D iDEP devices fabricated on a silicon substrate, we reported 50% selective trapping of 1 µm and 2 µm beads in a high conductivity 20.0 mS/m solution at 100 V_{DC} applied signal [19]. In this study, however, significant trapping of *S. aureus* bacteria at low signal amplitudes with electrodes capacitively coupled

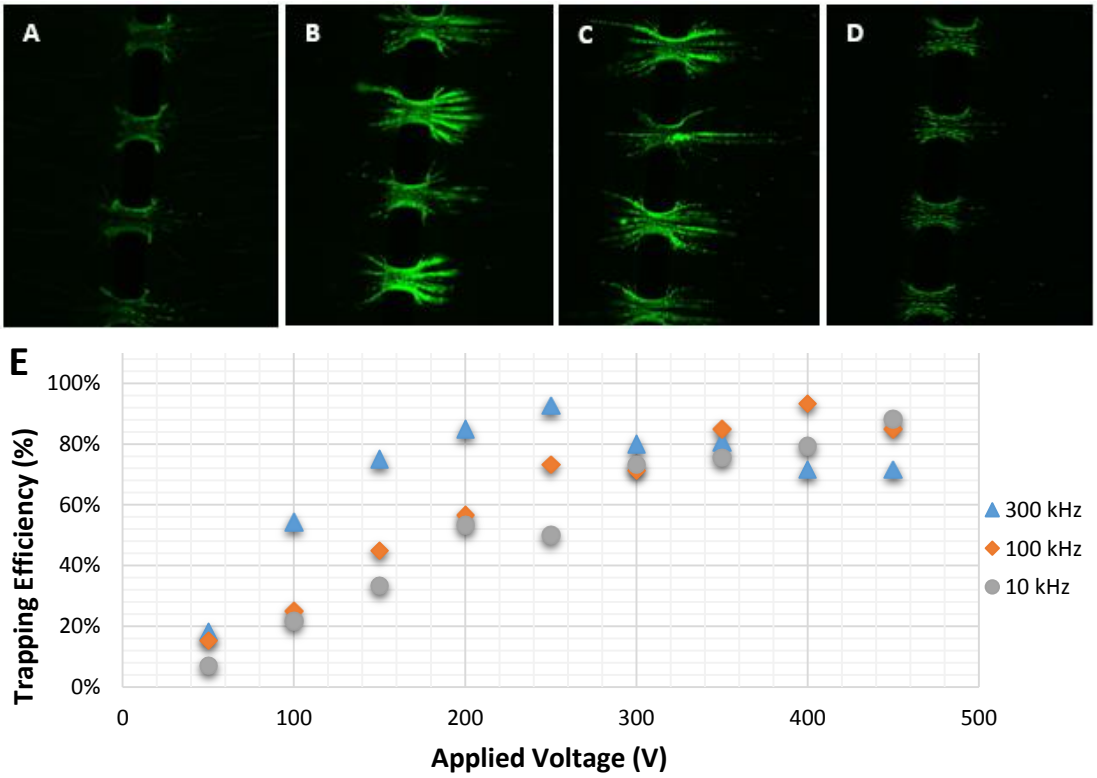

Figure 2.7: Low Voltage operation of the 3D DEP device (n=3). **A.** Poor trapping at 200 Vpp and 800 Hz applied frequency. **B.** Long pearl chains at low frequency 200 Vpp and 10 kHz. **C.** Reduced trapping along chains for 200 Vpp and 100 kHz applied signal. **D.** Trapping concentrated at the microposts 300 kHz. **E.** Trapping efficiency against varied applied signal voltages.

through a glass slide has been demonstrated. This 3D πDEP device achieves low voltage trapping while maintaining high trapping efficiency over a wide range of frequencies.

D. Flow Rate Analysis

Analysis to determine maximum throughput of the 3D πDEP device was conducted. The applied signal was held constant at 200 Vpp and 300 kHz, while the medium flow rate was varied from 20 µl/hr to 1000 µl/hr. Results showing capture efficiency as a function of fluid flow rate are shown in *Figure 2.8*. During the flow sweeps, it was observed that trapping improved with reducing fluid flow rates and this behavior is further supported by Equation 2.4. As shown in *Figure 2.8*, the device obtained 100% capture efficiency for flow rates up to 350 µl/hr and trapping efficiency over 90% for flow rates up to 700 µl/hr. The device capture efficiency decreased steadily from 700 µl/hr to 1000 µl/hr but remained above 50%. At these high flow rates, over 700 µl/hr, the drag force acting on the particles was significant to pull pearl chains of previously trapped *S. aureus* off the 3D microposts.

Notably, the 3D πDEP technology proposed in this work uses 3D insulating features. The constriction regions near the insulating posts are shallow as shown in the SEM image in Figure 4C-D. This ultimately compromises device throughput as opposed to 2D iDEP and eDEP devices that have been reported to operate at high flow rates [34, 35]. The 3D πDEP throughput could be readily enhanced by aligning channels in parallel or increasing

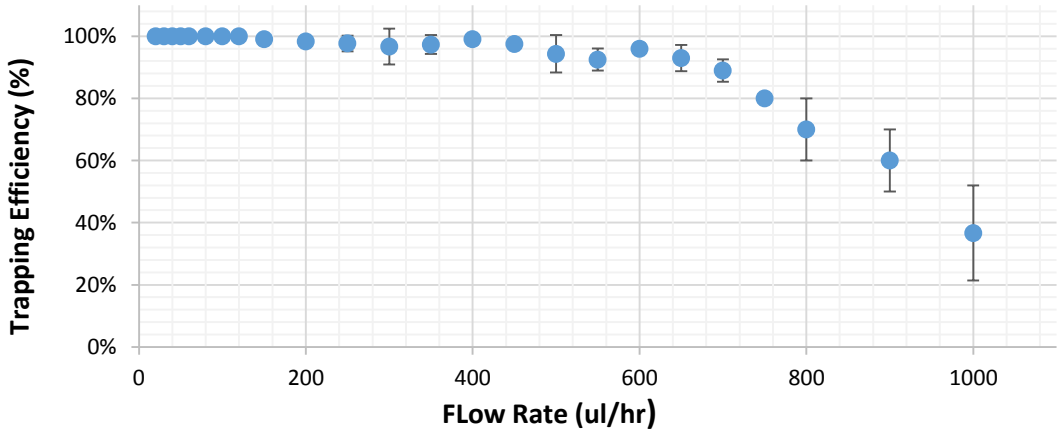

Figure 2.8: Observed DEP trapping of S. aureus by a 3D πDEP device at an applied electrical signal of 200 Vpp and 300 kHz. Capture efficiency as function of medium flow rate (n=3).

the channel depth and width dimensions. Consequently, the trapping efficiency deteriorated from here onwards. Therefore, for experiments with an emphasis on high trapping efficiency, flow rates under 700 μl/hr are preferable whereas in cases where high throughput is of greater importance, the device can operate above 700 μl/hr.

E. Separation of Particles

Biological samples containing live only, dead only, and a mixture of live/dead *S. aureus* bacteria were analyzed using the 3D πDEP device. A solution containing both live and dead *S. aureus* was used to investigate the ability of 3D πDEP to selectively concentrate closely related biological samples. The *S. aureus* dead sample was prepared by boiling a live bacteria sample in a water-bath at 80 ^{o}C for 20 minutes. The sample was allowed to cool for 5 minutes in a beaker of cold water and then stained red with a live/dead viability Kit (Backlit Invitrogen). This was then added to a similarly stained green live bacteria sample. Results from the mixed live/dead sample showed that we could separate live from dead bacteria at frequencies ranging from 30 – 60 kHz. *Figures 2.9A-B* show that with an applied signal of 400 Vpp and 30 kHz, 98% of the green stained live bacteria are trapped at the 3D microposts while the red stained bacteria can be seen escaping on the left side of the microposts.

Pointedly, we observe that with increased trapping of live bacteria, the electric field gradients in the channel rapidly increase especially when long pearl chains of bacteria are trapped at the microposts. This increases device capability to trap both live and dead bacteria. Dead bacteria start to accumulate on the previously trapped live bacteria pearl chains. However, when the applied signal is removed, the green bacteria that were strongly immobilized by the DEP force are immediately released as shown in *Figure 2.9C*. Dead bacteria previously trapped on the long pearl chains of live bacteria are released a few seconds later as shown in *Figure 2.9D* (see Appendix 2 for the video) [19]. This affirms our understanding that the live bacteria were selectively trapped at the frequency ranges 30 – 60 kHz while most of the dead bacteria escaped. We observed 100% capture efficiency when trapping a combination of live and dead *S. aureus* over a 90 –100 kHz frequency range as shown in *Figure 2.9H*. Trapping deteriorated beyond

400 kHz due to bandwidth limitations of the amplifier. It should be noted, however, that dead bacteria had a tendency to foul the surface and stick to the microposts even after the applied signal was removed as seen in *Figure 2.9D*. Fouled bacteria can be removed by increasing the flow rate prior to the next run.

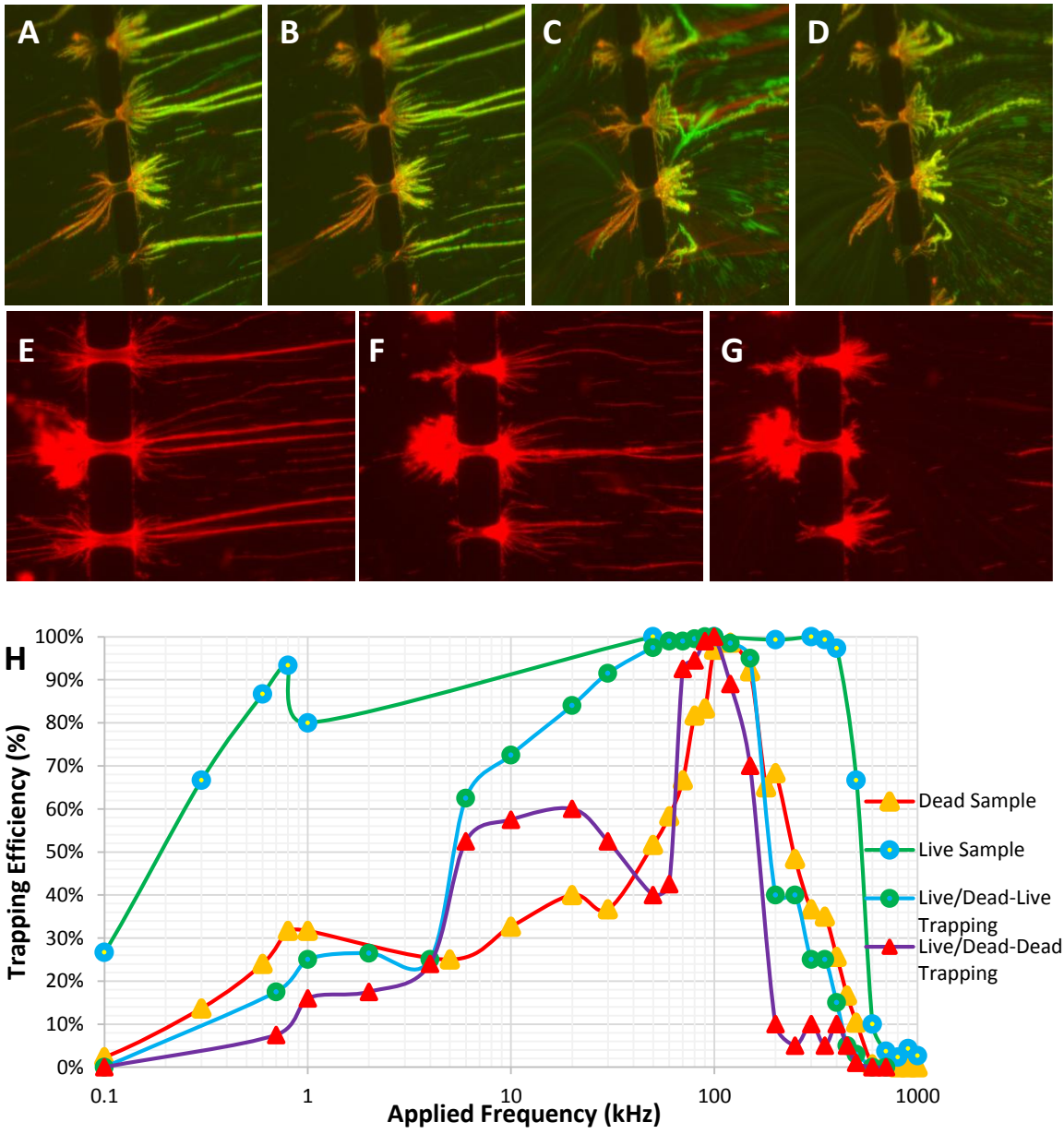

Figure 2.9: Sample of live and dead bacteria at 400Vpp and 100ul/hr. **A, B.** Selective trapping of live bacteria while the dead escape at 30kHz. **C.** Applied signal is removed and the live bacteria is immediately released. **D.** All bacteria is released though some fouls at the posts. **E, F.** Long pearl chain formed while trapping a dead bacteria sample at 50kHz and 100kHz. **G.** Trapping at 300kHz concentrated at the microposts. **H.** Superimposed results from purely live, purely dead and mixed live/dead bacteria frequency runs. (n=3)

As seen previously with live *S. aureus* samples, *Figures 2.9E-G* show trapping of dead bacteria with extra-long pearl chains formed at lower frequencies, 10–100 kHz. At higher frequencies (<250 kHz), the trapping was concentrated at the microposts due to the particle experiencing a stronger DEP force. To fine tune selectivity of the device, a frequency sweep for a purely dead *S. aureus* sample was obtained and interposed this with results from a purely live sample as shown in *Figure 2.9H*. The live sample (Green) consisted of only live bacteria. Results showed a trapping efficiency over 80% for frequencies ranging from 600Hz to 400 kHz and maximum trapping efficiency starting at 60 kHz. The more bacteria are trapped in elongated pearls, the more the electrical field gradient is enhanced within the channel further increasing the trapping efficiency. Notably beyond 400 kHz, the power amplifier starts to attenuate causing a sudden drop in the trapping efficiency. The same is true for Dead sample containing dead bacteria. However, we can easily observe that increase in the trapping efficiency of dead bacteria happens closer to 100 kHz and there is distinct efficiency between live and dead sample when it comes to frequencies between 1-70 kHz.

The Live/Dead sample consisted of a mixture of live and dead bacteria. Using ImageJ, we analyzed the trapping efficiency of live (Blue) and dead (Purple) bacteria in the mixed sample population. It should be noted that trapping can affect the local electric field gradient and hence, the trapping efficiency observed for the dead bacteria in the mixed population can be influenced by the trapping of live bacteria that can happen at lower frequencies. Nevertheless, we can see a more distinct separation between the live and dead bacteria at frequencies close to 60 kHz while at frequencies around 100 kHz, the trapping efficiency of the entire sample is close to 100%. Again, due to limitations in the power amplifier, we could not conclude if the chip is capable of efficiently separating the live and dead bacteria at higher frequencies.

2.5 Discussion and Conclusion

In this paper, we have introduced the first reported 3D πDEP device capable of achieving high capture efficiencies and separation of biological particles at low voltages and have showcased its performance through numerical models and experiments. 3D πDEP

combines the benefits of iDEP, eDEP and microstructures fabricsated in three dimensions. It is an advancement of our previously reported 2D iDEP and an alternative to our 3D iDEP device [20, 23]. As demonstrated in our results, 3D structures generate stronger DEP forces in comparison to 2D microstructures in iDEP devices and the passivated electrodes are reusable. The stronger electric field gradient generated is further supported by the theory presented earlier in Equation 2.1 showing that the $\mathbf{F}_{DEP}$ is a function of the electric field gradient $\nabla(\mathbf{E} \cdot \mathbf{E})$. 3D insulating structures increase this component and ultimately generate stronger DEP forces. As a result of stronger electric field gradients, the operating bandwidth of the device was greatly improved. Exploiting this wide operating bandwidth and the frequency dependent response of biological particles in a DEP device, we can obtain finer tuning when manipulating closely related samples. Consequently, stronger DEP forces allowed for trapping at lower applied voltages thereby minimizing complications arising from joule heating. Electrodes located

DEP Device	2D iDEP	3D πDEP
Advantages	- Insulating structure design flexibility	- High electric field gradients generated
	- Easy to mass produce	- 3D Flexibility in insulating structure design
		- No direct electrode contact with the sample
		- Low cost mass production of polymer substrate
		- Minimal heat buildup near insulating structures
		- Flexibility in electrode shape design
		- Large Bandwidth
Disadvantages	- Large heat buildup near insulating structures	- High AC fields to capacitively couple through glass slide
	- Electrodes in contact with solution	- 3D fabrication required
	- Requires large DC voltages to operate	

Table 2: Summary of advantages and disadvantages of 2D iDEP, 2D OπDEP, and 3D πDEP chip designs.

within the vicinity of the 3D microstructures reduce path travelled by current when the applied signal is turned and ultimately minimize heat buildup in the entire microfluidic channel. Heat buildup in the microfluidic channel can result in device failure [27] and potentially reduce sample viability in biological applications. Therefore 3D πDEP devices can be operated for longer durations with minimal temperature effects on the biological sample. Additionally, by capacitively coupling through an insulating layer, the electrodes are never in direct contact with the solution thus avoiding sample contamination and gas evolution. These reported advances in performance are obtained while maintaining a simple, low cost, single etch, single mask, polymer mold fabrication. The device ability to operate at lower applied voltages minimizes chances of cell death due to electroporation. To further curb this problem, the applied signal was turned on in short bursts during trapping and turned off after. The channel design of 3D insulating microstructures improves the electric field gradients, ultimately increasing the DEP force acting on bioparticles. Capture efficiency of 100% was achieved for an applied voltage of 200 Vpp over a wide frequency bandwidth ranging from 600 Hz – 400 kHz. Because trapping of microparticles is concentrated at the microposts, the device throughput can be improved by widening the microchannel. To characterize different biological samples, the applied signal amplitude and frequency as well as a combination of AC and DC signals can be manipulated to selectively trap bioparticles. Moreover, the 3D πDEP devices can be customized by changing the electrode and 3D insulating structures to achieve high selectivity of closely related bioparticles. This 3D πDEP device offers the capability for low cost disposable testing of water samples in the field. Additionally, the low frequency operation of the device allows for exploitation of a wider frequency range on the DEP spectrum when investigating different biological samples. A summary of the advantages and disadvantages of 2D iDEP and 3D πDEP microfluidic designs are shown in Table 2.

The reported results showcase the promising potential of the 3D πDEP device as a low cost, high throughput and highly efficient platform for biological sample analysis for applications ranging from pathogen manipulation to medical and therapeutic diagnostics. Furthermore, the passivated electrodes offer reusability and flexibility in electrode design.

3.0 TRAPPING OF SUBMICRON PARTICLES USING 3D EMBEDDED-ELECTRODE INSULATOR-BASED DIELECTROPHORESIS

This work was presented in a poster at the Biomedical Engineering Society (BMES) annual meeting, 2014. BMES serves as a leading society and professional home for biomedical and bioengineering research.

3.1 Introduction

Submicron bioparticles such as protein, yeast, bacteria and viruses can be detected, manipulated and characterized using dielectrophoresis [36]. Using positive dielectrophoresis, researchers have successfully demonstrated nanoparticle manipulation by precipitating DNA and protein samples [37]. Integration of this DEP technology onto a lab on a Chip system capable of analyzing virus-sized particles would avail a low cost diagnostic tool.

In this study, we present for the first time a 3D embedded-electrode insulator-based dielectrophoresis device (3D iDEP) used to detect and trap submicron particles (0.5µm beads). The device has 3D insulating features that increase the electric field gradient in the microchannel and ultimately generate stronger DEP forces [9, 38]. Device performance is complimented by the embedded electrodes passivated by a thin layer of polydimethylsiloxane (PDMS) polymer. This allows for device activation within the vicinity of the microposts without favoring heating effects that arise when the electrodes are in direct contact with the solution [19]. Submicron particle trapping efficiencies < 90% are reported over a wide frequency range of 2 kHz – 300 kHz at 0.1 µl/hr and 300Vpp.

3.2 Theory

Dielectrophoresis is the motion of neutrally charged polarizable particles due to a non – uniform electric field. Polarization occurs when the distribution of charge within a particle is distorted due to an external field. Dielectrophoretic behavior of the particle is dependent on size and the electrical properties of the particle. It's on the basis of this concept that selectivity can be achieved using dielectrophoresis (DEP). The time average DEP force acting on a particle in an electric field, **E** is given by:

$$F_{DEP} = 2\pi R^3 \varepsilon_m \,\mathrm{Re}\left[f_{CM} \right] \nabla \left(\mathbf{E} \bullet \mathbf{E} \right) \quad (3.1)$$

where R is the particle radius, Re [f_{CM}] is the real part of the Clausius-Massotti factor. f_{CM} is a measure of the polarizability of a particle and it is given by:

$$f_{CM} = \frac{\left(\varepsilon_p{}^* - \varepsilon_m{}^* \right)}{\left(\varepsilon_p{}^* + 2\varepsilon_m{}^* \right)} \quad (3.2)$$

where ε_p * and ε_m * are complex permittivities of the particle and medium respectively. f_{CM} not only depends on complex permittivities but also on the frequency of the applied signal. This accounts for the DEP force varying with frequency. The real part of f_{CM} varies from (1 < Re [f_{CM}] < - 0.5 and will therefore generate a positive or negative DEP force.

Particles in microfluidic systems will also experience a drag force given by Stokes law:

$$\boldsymbol{F}_{Drag} = -fv \quad (3.3)$$

where *f* is the friction factor of the particle. For low Reynold numbers, the friction factor of spherical particles is:

$$f = 6\pi\eta r \quad (3.4)$$

Not accounting for Brownian motion and the buoyancy force, the equation of motion for the particle in a DEP microfluidic system is given by:

$$m\,\frac{dv}{dt} = \boldsymbol{F}_{DEP} - \boldsymbol{F}_{Drag} \quad (3.5)$$

3.3 Materials and Methods

The device is fabricated using our in-house single-mask process for 3D fabrication technique [30]. Using RIE lag, features of varying depth and width are etched in silicon and reverse features are created on a glass substrate as shown in *Figure 3.1C-D*.

A photo-mask layout consisting of an array of rectangular openings with different sizes and aspect ratios is designed in Layout-Editor. Thereafter photoresist is patterned and the pattern is transferred to the oxide. The DRIE etch exposes creates 3D silicon features using an isotropic etch. The reactive ion etch lag (RIE lag) and its dependency on the geometrical patterns of the mask layout is exploited to create 3D cavities and microposts. This technique provides three-dimensional flexibility over structure formation. Subsequently, photoresist is stripped and the silicon substrate is bonded to a Pyrex wafer under vacuum. The Pyrex wafer is melted under a furnace to form a glass mold. The glass

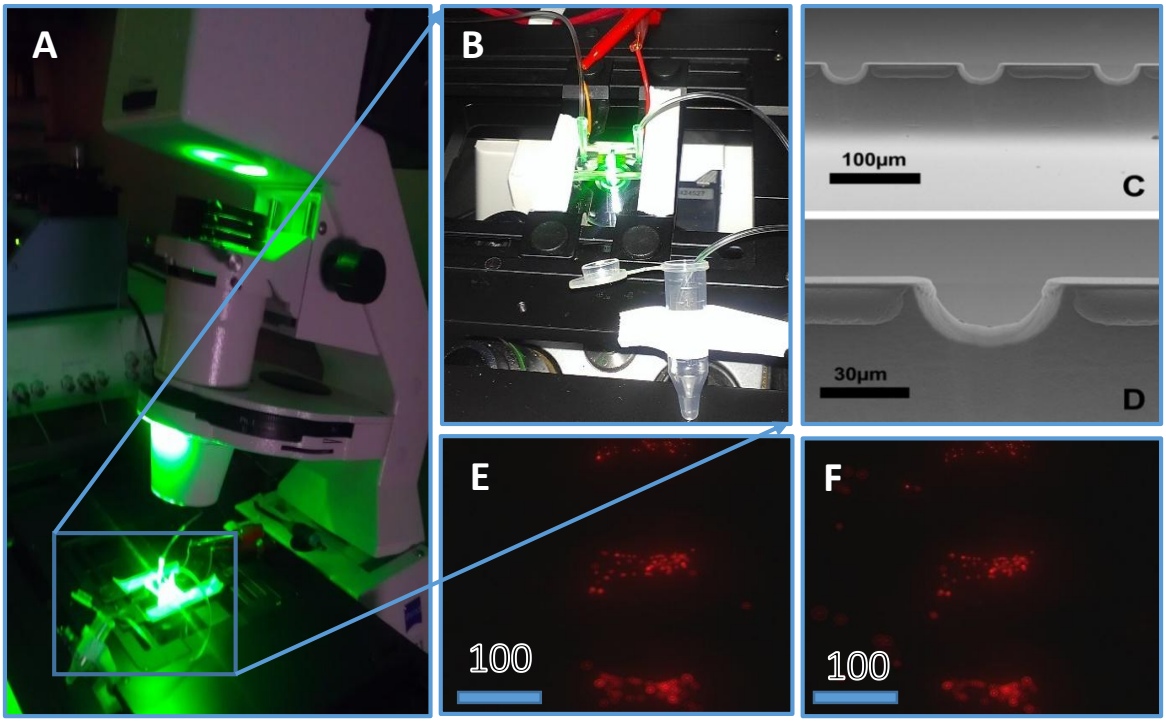

Figure 3.1. A-B. Experimental setup **C-D.** SEM images depicting the 3D insulating micropost **E-F.** Images exhibiting trapping and release of submicron beads

substrate master mold is left behind after the silicon substrate is etched away using KOH etch procedure. Low cost PDMS devices are mass produced using the glass master mold. The multiple device PDMS polymer are carefully peeled off the mold, cut into single devices, and 2 mm holes are punched into the microfluidic channels for fluidic ports. The devices are sealed by plasma bonding, using a Plasma Cleaner (Harrick Plasma), to a glass cover-slide (Electron Microscopy Sciences) forming the microfluidic cartridge.

Sub-micron (0.5 µm) beads were suspended in DI water with a measured conductivity 800 µS/m. The experimental setup is as shown in *Figure 3.1A-B*. The microfluidic cartridge is mounted onto the Zeiss inverted microscope (Model - Z100) stage and secured in place using paper tape. A 1 ml syringe containing suspended sub-micron beads is then fitted onto the syringe pump and connected to the 3D πDEP device inlet port. As shown in *Figure 3.1B*, tubing is connected from the outlet port to waste microtube. Submicron particles are pressure driven through the device using a Harvard Apparatus syringe pump at 0.1 µl/hr. 300 Vpp AC voltage signal is applied across the microposts to activate the device. A frequency sweep ranging from 10 Hz – 450 kHz is conducted and trapping efficiency is measured. Extracted results of trapping efficiency are shown in *Figure 3.2*.

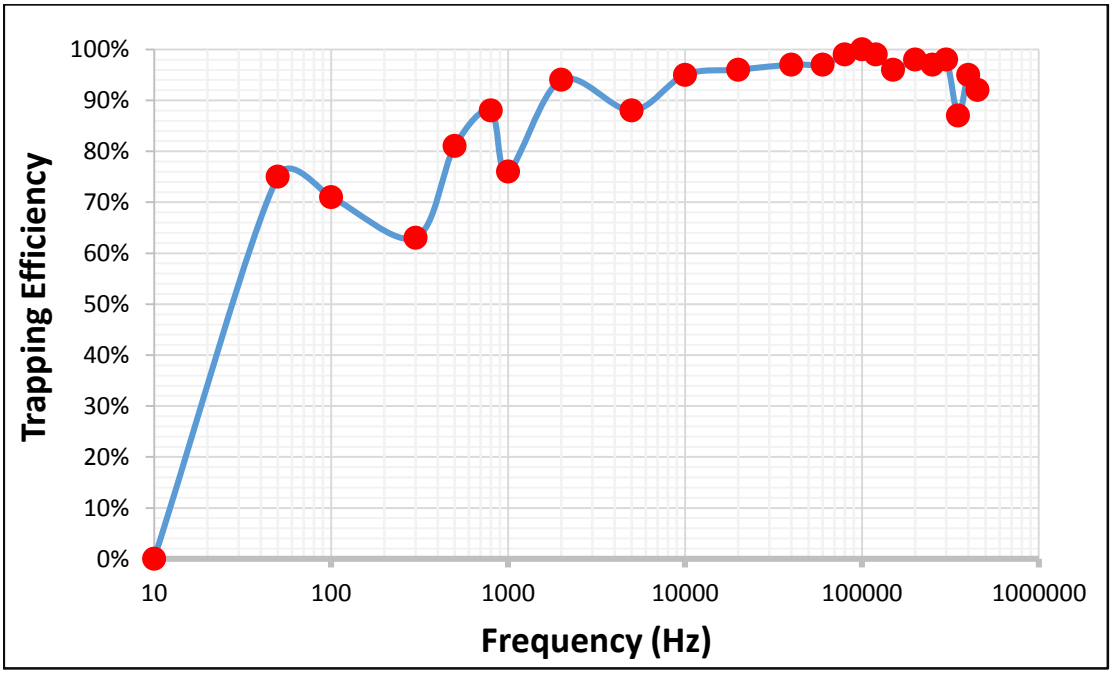

Figure 3.2. Sub-micron bead frequency sweep showing trapping efficiency.

3.4 Results and Discussion

In this work, trapping of submicron particles at trapping efficiencies over 90% is demonstrated over a wide frequency range. With insulator based dielectrophoresis devices (iDEP), DEP forces are generated due to non-uniform electric field gradients at the insulating microposts. In this case, the 3D nature of the insulating posts increases the electric field gradients, and as a result stronger DEP forces are generated. When the applied signal is turned on, the submicron beads are observed to trap at the 3D insulating microposts as shown in *Figure 3.1E*.

In *Figure 3.1F* the signal is turned off and the beads are released to the left hand side of the posts. In *Figure 3.2*, results show the device's capability to operate with high trapping efficiency even at low applied frequencies. The frequency sweep shows high trapping efficiency over 90% for applied signals ranging from 2 kHz – 300 kHz and greater than 60% trapping efficiency for lower frequencies between 50Hz - 1000Hz. This is demonstrates the wide frequency range operation of 3D iDEP. Additionally, because the electrical properties beads do not change significantly as the frequency changes, these results further support that concept. However, due to slight changes is surfaces properties of the beads at different frequencies, variations are reported. The particle size and magnitude of the generated electric field gradient play a bigger role in determining the DEP force experienced by the sub-micron particles.

This work demonstrated the ability to detect and trap sub-micron particles. Results presented point to the capability of implementing 3D iDEP devices that can successfully detect, trap and characterize submicron particles with biological applicability. Real life submicron sized bioparticles like viruses, DNA, protein, chromosomes, and bacteria could be analyzed with further advancement in this technology. The unique electrical properties of the bioparticles would facilitate selective trapping of closely related samples.

4.0 HIGH THROUGHPUT 3D iDEP

4.1 Introduction

In 3D πDEP systems, microparticles are trapped and isolated using insulating microstructures. Due to the nature of enhanced graduate profiles of the insulating structures, the throughput capability of the device is compromised. Considering that most real life sample populations are in relatively large volumes, it is beneficial to further enhance 3D iDEP device performance by increasing device throughput.

One of the ways that device throughput can be improved is by designing multiple iDEP microfluidics channels in parallel. This would ultimately increase throughput by a factor of the number of channels added. In this case, device throughput is increased without compromising device trapping efficiency. Alternatively, increasing microchannel width and height dimensions would also increase device throughput. However this would be at the expense of device trapping efficiency. Furthermore, increasing the external fluid pump pressure would also increase device throughput. This case, however, adversely increases the drag force acting on the bioparticles and stronger DEP force would be required to achieve the same trapping efficiency.

4.2 Methods and Materials

Configurations of high throughput 3D iDEP devices have been investigated and the designs are shown in *Figure 4.1* below. Devices were fabricated using our in-house developed 3D micromachining technique discussed in Chapter 2 [31].

Briefly, a silicon wafer is patterned with photoresist and etched using an Alcatel AMS-100 Deep Reactive Ion Etcher (DRIE) to obtain 3D insulating structures. A Pyrex wafer is anodically bonded to the etched silicon wafer under vacuum. The glass mold is then cured in a heated chamber after which the silicon wafer is stripped using a KOH procedure. Liquid PDMS is poured onto the glass mold and cured. Finally, the PDMS is plasma bonded to a cover glass to form the microfluidic cartridge. *Figure 4.3* shows the fabricated devices. The operating principle of these devices is to concentrate the bacteria

at the insulating microposts and also increase throughput via multiple operating microchannels. The electric field gradient current is concentrated through the constriction

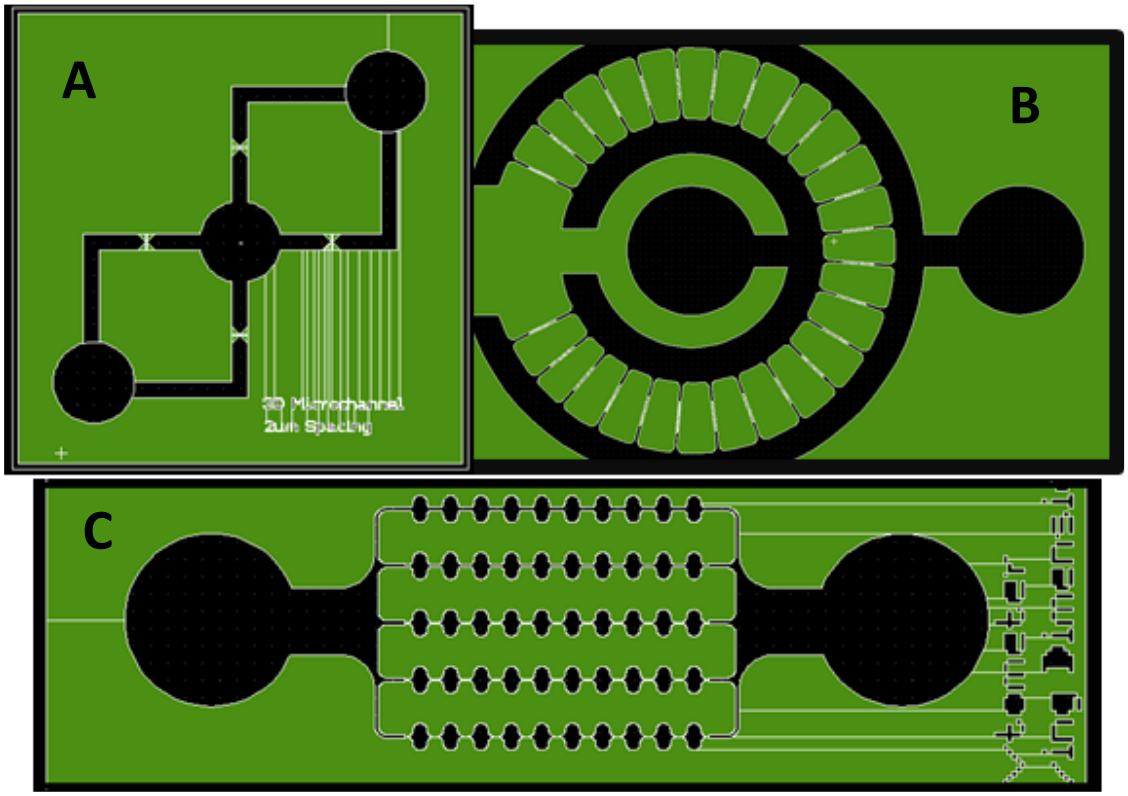

Figure 4.1: Proposed high throughput 3D iDEP designs.

generating the strongest DEP forces at the 3D constriction microchannels. The 3D iDEP high throughout system is consequently more DEP sensitive in the at the constriction microchannels then elsewhere in the channel.

Figure 4.1A shows a four-armed, high constriction ratio design with enhanced width and depth dimensions. This is a combination of parallel microchannels and increased geometry dimensions to achieve improved throughput performance. *Figure 4.1B* shows a radial design that optimized device area with multiple microchannels connected to single input and output ports. Below is *Figure 4.2* showing SEM imagery of the 3D dimensionality of the fabricated microchannels in silicon from the layout design in *Figure 4.2B*. SEM imaging shown *Figure 4.2* vividly highlights the 3D control over device geometry obtained using our in-house 3D micromachining technique [31]. Further, the fabricated PDMS devices are bonded to glass wafers to form microfluidic

cartridges. *Figure 4.3* shows images of the microfluidic devices as seen under an inverted microscope. *Figure 4.3A* shows the high-constriction channel within the vicinity of the electrodes from the design in *Figure 4.1A. Figures 4.3B-C* show enhanced images from the round cytometer device in *Figure 4.1B.*

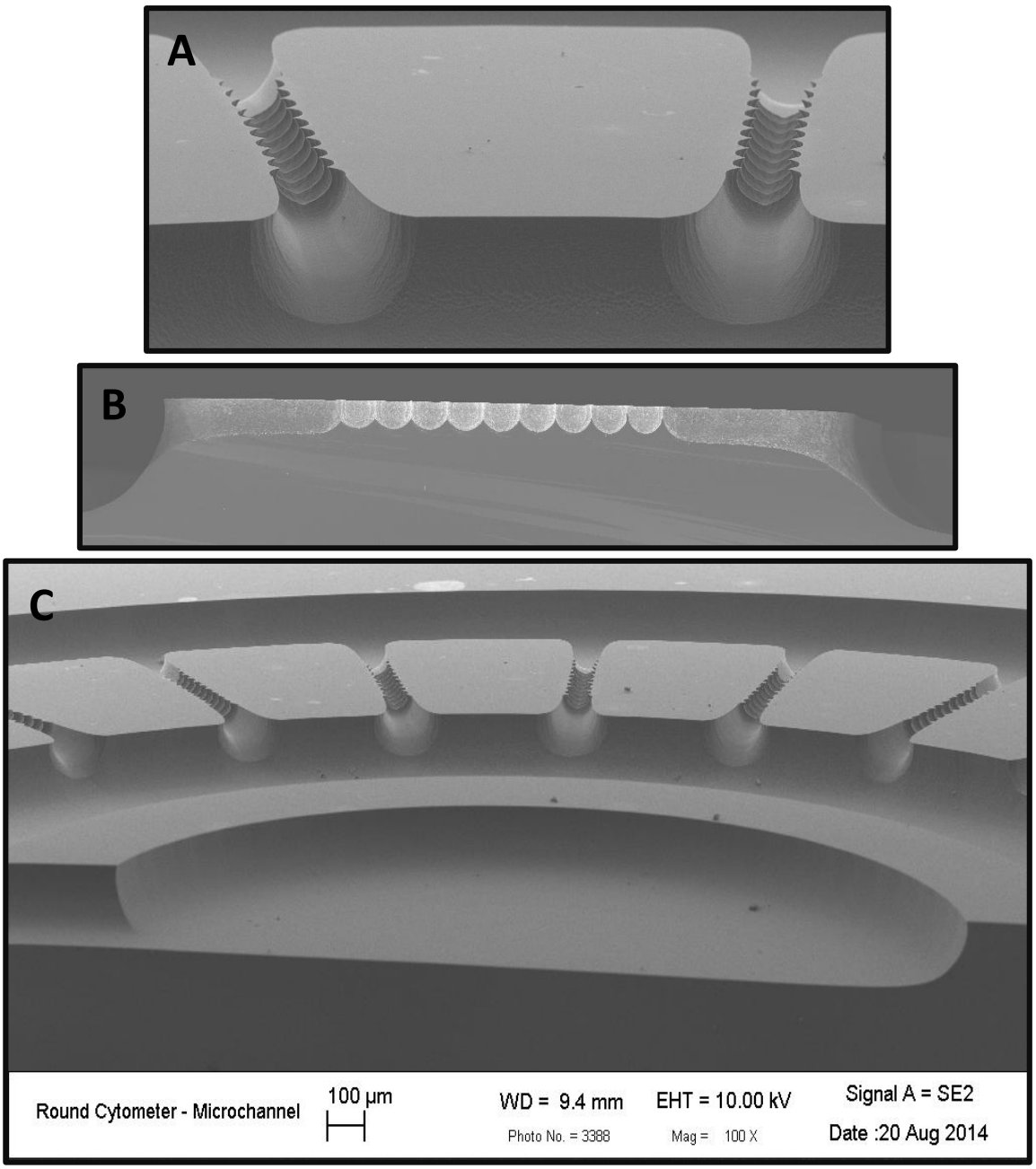

Figure 4.2. SEM imaging of the round cytometer high throughput 3D iDEP microchannels in silicon. **A**. Enhanced imaging of two parallel microchannels. **B.** A slice image of a single microchannel **C**. Half of the microfluidic device showing the inlet

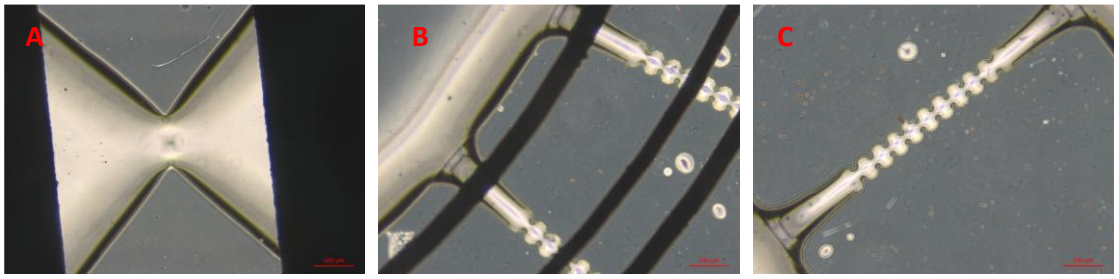

Figure 4.3: Images showing high throughput 3D iDEP microfluidic cartridges after bonding with embedded electrodes.

4.3 Results and discussion

The device was tested by suspending bacteria in de-ionized water of measured conductivity 800 µS/m. The experiments were conducted on *Staphylococcus Aureus* (*S. aureus*) strain (ATCC 12600) cultured in brain heart infusion media (Bactrius Limited, Houston TX). *S. aureus* cells were cultured in 100 ml of broth medium at 37 °C and 165 rpm to the exponential growth phase (OD600 ~ 0.8).

During device operation, the solution was passed through the device with a syringe pump. Using an amplified AC voltage signal, the electrodes were activated for 40-60 second runs during the experiment. *Figure 4.4* shows the frames of a recorded video of the experiments. First, the bacteria is infused through the inlet of the 3D iDEP high throughput device at 300 µl/hr for a single microchannel as shown in *Figure 4.4A*. Bacteria can be seen to flow from the lower right corner inlet port, through the parallel microfluidic channels, and out in rings in the outer main microfluidic channel. When the electrical signal of 350Vpp at 100 kHz is applied, the bacteria are concentrated at the microposts for set period of time and this can be seen in *Figure 4.4B*. Notably, because only one half of the device was activated at a time, images clearly show enhanced trapping on one half of the device. Observably, some bacteria was seen to stick on the walls of the inactivated half of the device, however, this was minimal as most of the bacterial was observed escaping. Then the bacteria is released when the applied signal is turned off in *Figure 4.4C*. Clumps of previously trapped bacteria can be seen escaping.

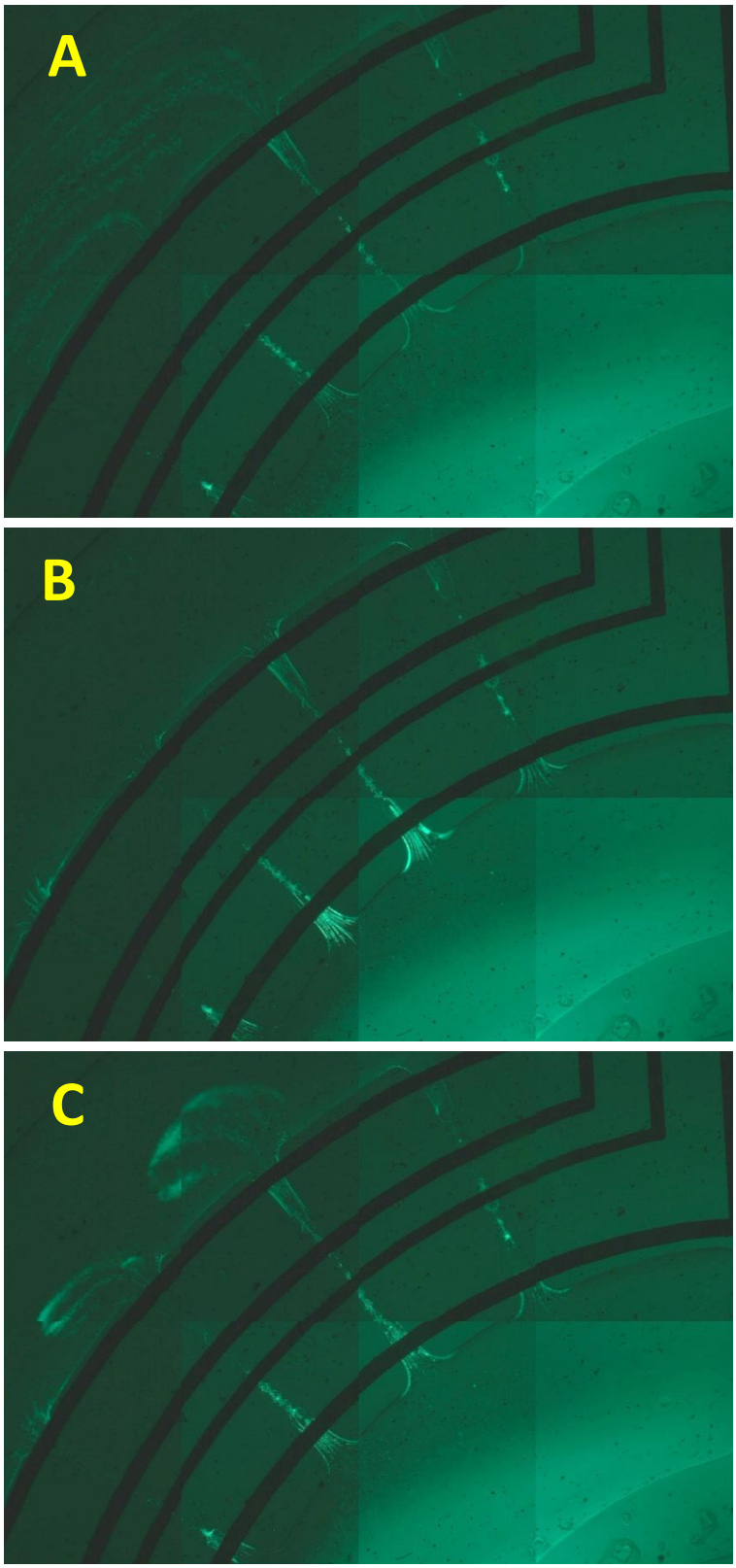

Figure 4.4. 3D iDEP high throughput device analysis. **A**. bacteria is infused through the channel. **B.** Applied electrical signal is turned on and bacteria is trapped **C**. Bacteria is released when the signal is turned off

4.4 Outlook and Conclusion

These results demonstrate that it is possible to improve iDEP device throughput performance without compromising DEP trapping efficiency. These reported results were conducted at 300 µl/hr, which is three times the flow rate reported in our previous experiments [39]. This is without accounting for the 28 parallel microchannels that increase the volume of the constriction insulating microstructures. These parallel microchannels ultimately increase the overall device throughput per run. Notably, the device geometry also maximizes device area with a single inlet in the middle of the device and a single outlet for all parallel microchannels.

It may be possible to improve the DEP performance of this system by incorporating 3D insulating posts. The current device design exploits sinuated 3D microchannel walls to generate non- uniform electric field gradients. 3D insulating posts would further increase the electric field gradient generated and therefore increase the DEP force generated.

Additionally, the device could be made more robust by eliminating the reference electrode pairs that were added for multi-frequency or zone analysis. Results showed that these interfered with the electric field gradient when inactivated by acting as an insulating structure in the channel. Different zones could be investigated by designing different electrode designs and then investigated these individually. Alternatively, passivated electrodes with multiple electrode combination were less susceptible to interfering with the system when inactivated.

5. CONCLUSIONS AND FUTURE WORK

5.0 Summary of Results

In this work, an in-house developed technique is used to fabricate microfluidic devices that exploit the physics of three-dimensional insulator based dielectrophoresis (3D iDEP) to characterize, analyze and isolate bioparticles. These discussed systems employ large constriction ratios of 3D fabricated channels to generate high electric field gradients and ultimately stronger DEP forces in comparison to traditional two dimensional (2D) systems. Consequently, the trapping and characterization capability of small, closely related microparticles is made feasible. In Chapter 2, it has been demonstrated that device performance is significantly improved by 3D insulator based devices in comparison to 2D iDEP devices.

Despite tremendous progress in the field of iDEP over the recent years, commercialization still poses a daunting task due to the high costs associated with these systems. Most of this has been attributed to costly fabrication procedures accompanied by expensive supporting equipment used. The fabrication techniques presented in this work are yet another step in the right direction. A single DRIE etch step is used to create 3D features with a single mask. Furthermore, microfluidic devices are batch fabricated in low-cost PDMS polymer.

Even more importantly, millions of lives are affected every year as a result of waterborne pathogens and microbial diseases. While solutions to this problem may exist today, many of the current technologies are expensive and inapplicable to all regions of the world. In this work, MEMS technology is employed to advance existing systems or offer alternative accessible solutions through highly efficient, low-cost pathogen detection MEMS systems.

5.1 Pulsed iDEP trapping

5.2.1 Introduction

Controlled trapping and separation of microparticles in microfluidic devices is very important especially because of its potential application in the analysis of bioparticles.

DEP provides the controllable, selective and accurate manipulation of microparticles by varying the voltage, frequency, or phase of the applied electric signal. So far, most of the traditional iDEP systems utilize a single applied voltage to trap and isolate bioparticles at the insulating posts of the microchannel.

The ability to combine the benefits of iDEP and pulsed electric fields presents yet another avenue to investigate. By applying a pulsed electric field to activate the device, the generated DEP force acting on the bioparticles is also pulsed. This therefore generates a time-varying DEP force that is continually competing with a constant drag force acting on the particle. *Figure 5.1* shows an image where particles respond uniquely to a pulsed electric signal in an eDEP microfluidic system [40]. For previously trapped particles to be retained at the trapping posts when the applied electric signal is turned on, the Stokes force acting on the particles has to be less than the peak DEP force.

Particles will experience a DEP force which when sufficiently strong will cause them to get trapped. They are then released when the electric pulse signal goes to zero and

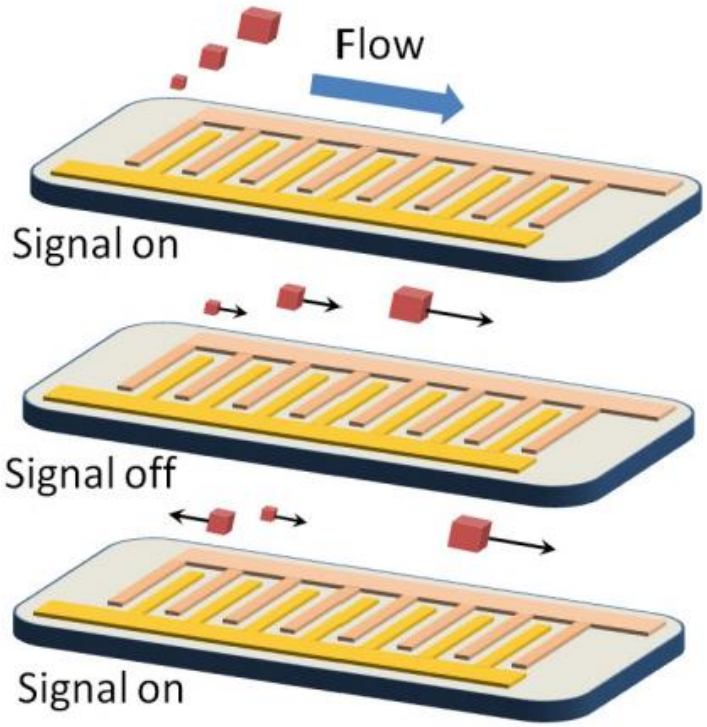

Figure 5.1. Uniquely responding particles to a pulsed electric signal in an eDEP microfluidic system. *K. Khashayar, et al. Dielectrophoretic platforms for bio-microfluidic systems. Biosensors & Bioelectronics 26.5 (2011). Used with permission of Elsevier, 2015.*

continue to move through the channel due to a mechanically or electrically induced drag force. Different particles of varying shapes and sizes experience different fluid forces and consequently acquire different velocities within the same medium. This causes the particles to end up at different locations within the channel over a given period of time. On this basis, closely related particles can be trapped and released at different rates allowing for them to be separated as they move through the channel. This concept is synonymous to chromatography. A combination of the selective behavior of DEP and the unique response to fluid forces can be exploited to enhance device performance.

An existing pulsed system by Hai-Hang Cui et al demonstrates tunable separation of particles of different sizes. Using a time varied DEP signal, the microfluidic DEP system successfully traps smaller particles while the larger ones are observed to escape. An analytical model explaining the dynamic behavior of particles under pulsed DEP is also presented in this study [41].

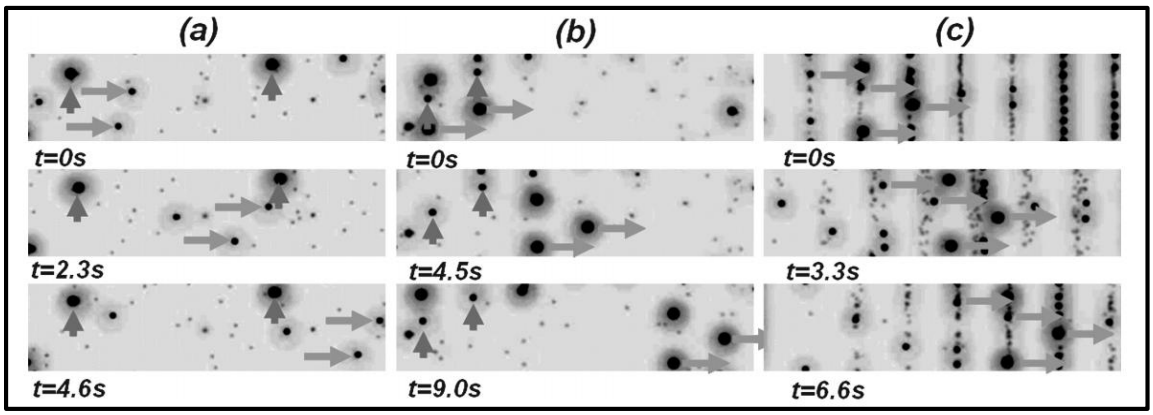

Figure 5.2. Pulsed eDEP trapping of different particle sizes. (a) At f= 2 Hz and V = 12 Vpp, 10µm beads are retained while 3µm and 5µm beads move downstream (b) At f= 1.05 Hz and V = 20 Vpp, 5µm beads are retained, while 3µm and 10µm beads move downstream (c) At f = 0.3 Hz and V = 20 Vpp, 3µm beads are retained, while both 5µm and 10µm beads move downstream. ↑ indicate stopped particles and → indicate forward moving particles.
Cui, Hai-Hang, et al. Separation of particles by pulsed dielectrophoresis. Lab on a Chip 9.16 (2009). Used with permission of the Royal Society of Chemistry, 2015.

While some researchers have investigated pulsed DEP systems, these have been focused on eDEP microfluidic systems [41, 42]. This work proposes a combination of iDEP and pulsed electric signals.

5.2.2 Methods and Materials

Varying novel constriction ratio designs for pulsed iDEP have been developed and the designs are shown in *Figure 5.3* below. The devices were fabricated using both 2D and 3D fabrication techniques.

A silicon wafer was patterned using photolithography and then selectively etched using a Deep Reactive Ion Etch (DRIE) process. Depending on the etch process, a 2D or 3D mold was created. This was then used to make a PDMS reverse mold. Prior to pouring the PDMS polymer onto the silicon mold, the silicon wafer was coated with

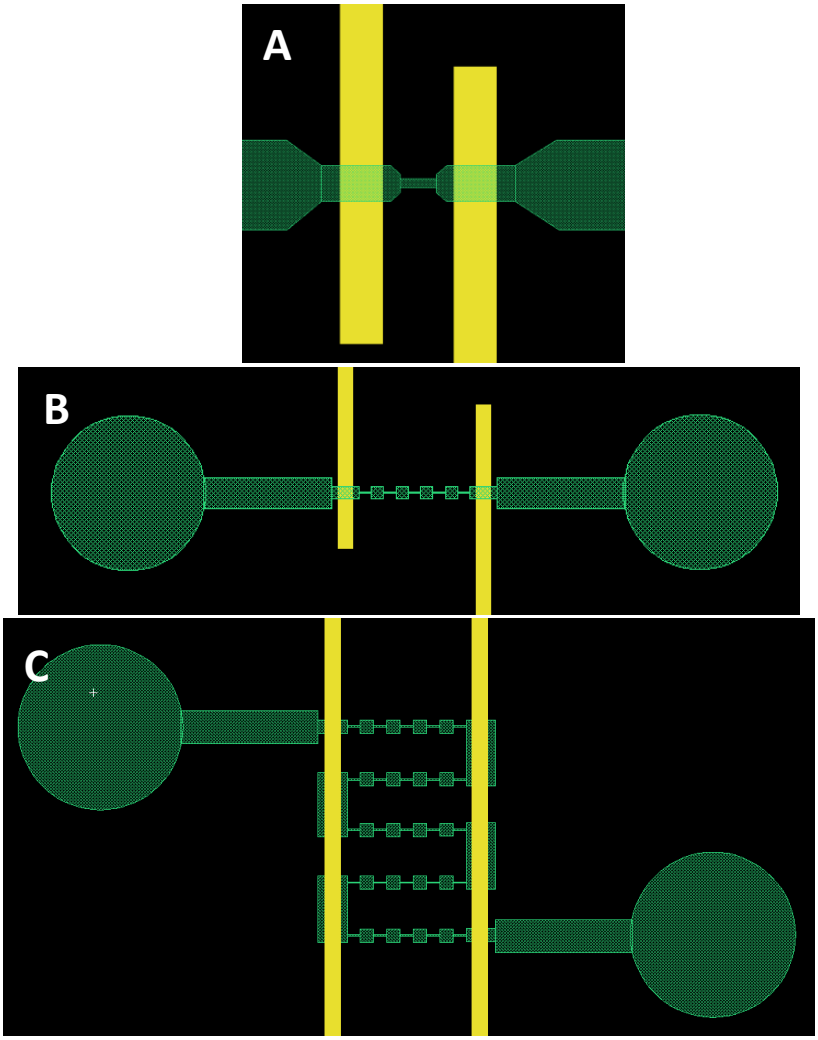

Figure 5.3. Pulsed iDEP device layout designs

Trichlorosilane in a gas chamber for one hour to prevent stiction. The PDMS mold was then cured and used to batch manufacture PDMS devices.

Figure 5.3A shows the enhanced constriction region for a short channel showing the yellow electrodes and the green section of the microchannel. In these designs, the electrodes are located in the vicinity of the constriction region to increase the localized electric field. In *Figures 5.3B* and *5.3C*, an elongated channel is designed to allow for the particles to travel some distance in between pulses.

5.2.4 Preliminary Results and Discussion

Preliminary investigation has been conducted using *S. aureus* bacteria as well as beads. The focus of the initial experiments was to test the DEP capability of the microchannels. A concentration of 1 X 10^9 cells/ml was used to investigate the DEP sensitivity of the insulating constrictions. *S. aureus* cells suspended in DI water were infused through the

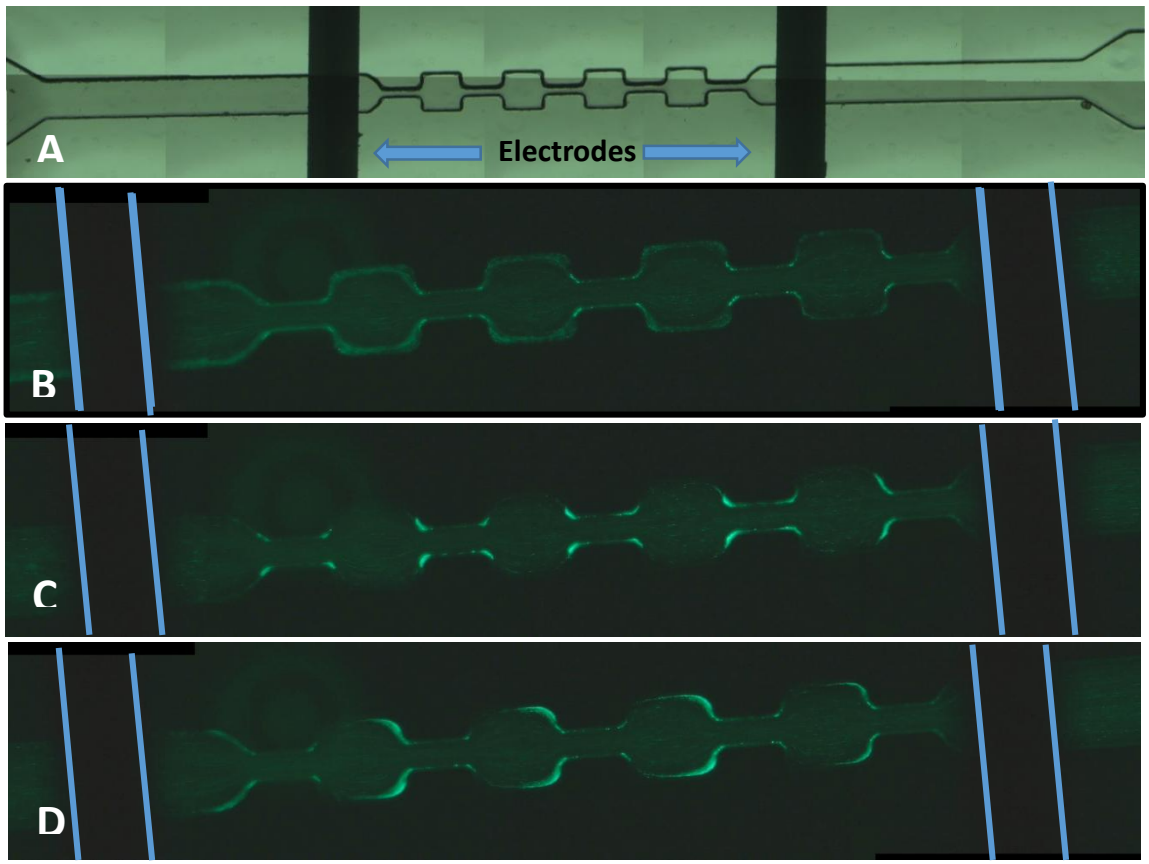

Figure 5.4. Pulsed iDEP device preliminary experimental results

2D microchannel at a flow rate of 20 µl/hr using a Harvard-Apparatus syringe pump.

The device shown in *Figure 5.4* was designed with 25µm constrictions and 100 µm wide regional zones along the microfluidic channel. During the DRIE etch process, these constriction channels are widened as seen in *Figure 5.4B.* Nonetheless, even with the diminished constriction ratio, results showed significant DEP device sensitivity.

Results showed that when the electric signal of 350Vpp and 100 kHz was turned on, the bacteria is trapped in the constriction areas as depicted in *Figure 5.4B*. Upon turning off the electric signal, the bacteria is released and can be seen transiting through the microchannel in *Figure 5.4D*.

5.2.5 Outlook and Conclusion

Observably, in an attempt to initiate pulsed-DEP trapping, the drag force acting on the bacteria was too strong that most of the previously trapped bacteria had already left the insulating microposts. During this study, results showed that pulsed DEP experiments would be better suited for low concentration samples. This way, the specific particle samples being investigated are better tracked as they move throughout the channel. Going forward, beads samples were investigated at a much slower flow rate (< 20 µl/hr) to allow for sufficient time to apply multiple pulses to the same particle sample.

The observation of trapping at the insulated constrictions is an encouraging step. In addition, low concentration samples would potentially make particle tracking in a pulsed DEP system easier. A proposed use of larger samples like beads and mammalian cells in low concentrations will further aid in this analysis. Additional testing of these proposed samples is needed before any conclusions can be drawn.

REFERENCES

1. World Health Organization, U.-W., UN-water global analysis and assessment of sanitation and drinking-water (GLAAS) 2014 - report. 2014.
2. Grabow, W., Waterborne diseases: Update on water quality assessment and control. *Water S. A.*, 1996. **22**(2): p. 193-202.
3. Medema GJ, P. P., Dufour A, Robertson W, Waite M, Hunter P, Kirby R, Anderson Y, *Assessing Microbial Safety of Drinking Water Improving Approaches and Methods: Improving Approaches and Methods*. 2003: OECD Publishing, World Health Organization.
4. Cabral, J. P., Water microbiology. Bacterial pathogens and water. *International Journal of Environmental Research and Public Health*, 2010. **7**(10): p. 3657-3703.
5. Maluf, N. and K. Williams, *Introduction to microelectromechanical systems engineering*. 2004: Artech House.
6. Bryzek, J., Impact of MEMS technology on society. *Sensors and Actuators A: Physical*, 1996. **56**(1): p. 1-9.
7. Whitesides, G. M., The origins and the future of microfluidics. *Nature*, 2006. **442**(7101): p. 368-373.
8. Pohl, H., *Appl. Phys.*, 1951. **22**: p. 869-871.
9. Nakidde, D., et al., Three dimensional passivated-electrode insulator-based dielectrophoresis. *Biomicrofluidics*, 2015. **9**(1): p. 014125.
10. Pohl, H. A., Dielectrophoresis -The Behavior of Neutral Matter in Nonuniform Electric Fields. *Cambridge University Press, Cambridge, UK*, 1978(Cambridge University Press, Cambridge, UK,).
11. Huang, Y., et al., Differences in the AC electrodynamics of viable and non-viable yeast cells determined through combined dielectrophoresis and electrorotation studies. *Physics in Medicine and Biology*, 1992. **37**(7): p. 1499.
12. Zhou, R., P. Wang, and H.-C. Chang, Bacteria capture, concentration and detection by alternating current dielectrophoresis and self-assembly of dispersed single-wall carbon nanotubes. *ELECTROPHORESIS*, 2006. **27**(7): p. 1376-1385.
13. Hunt, T. P. and R. M. Westervelt, Dielectrophoresis tweezers for single cell manipulation. *Biomedical Microdevices*, 2006. **8**(3): p. 227-230.
14. Shake, T., et al., Embedded passivated-electrode insulator-based dielectrophoresis (EπDEP). *Analytical and Bioanalytical Chemistry*, 2013. **405**(30): p. 9825-9833.
15. Davalos, R., et al., Performance impact of dynamic surface coatings on polymeric insulator-based dielectrophoretic particle separators. *Analytical and Bioanalytical Chemistry*, 2008. **390**(3): p. 847-855.
16. Martínez-López, J., et al., Characterization of electrokinetic mobility of microparticles in order to improve dielectrophoretic concentration. *Analytical and Bioanalytical Chemistry*, 2009. **394**(1): p. 293-302.
17. Sanchis, A., et al., Dielectric characterization of bacterial cells using dielectrophoresis. *Bioelectromagnetics*, 2007. **28**(5): p. 393-401.
18. Braff, W. A., et al., Dielectrophoresis-Based Discrimination of Bacteria at the Strain Level Based on Their Surface Properties. *PLoS ONE*, 2013. **8**(10): p. e76751.

19. Zellner, P. and M. Agah, Silicon insulator-based dielectrophoresis devices for minimized heating effects. *ELECTROPHORESIS*, 2012. **33**(16): p. 2498-2507.
20. Zellner, P., et al., 3D Insulator-based dielectrophoresis using DC-biased, AC electric fields for selective bacterial trapping. *ELECTROPHORESIS*, 2014: p. n/a-n/a.
21. Kale, A., et al., Numerical modeling of Joule heating effects in insulator-based dielectrophoresis microdevices. *ELECTROPHORESIS*, 2013. **34**(5): p. 674-683.
22. Sridharan, S., et al., Joule heating effects on electroosmotic flow in insulator-based dielectrophoresis. *Electrophoresis*, 2011. **32**(17): p. 2274-2281.
23. Zellner, P., et al., Off-chip passivated-electrode, insulator-based dielectrophoresis (OπDEP). *Analytical and Bioanalytical Chemistry*, 2013. **405**(21): p. 6657-6666.
24. Pohl, H. A. and J. P. Schwar, Factors Affecting Separations of Suspensions in Nonuniform Electric Fields. *Journal of Applied Physics*, 1959. **30**(1): p. 69-73.
25. Pethig, R., Review article—dielectrophoresis: status of the theory, technology, and applications. *Biomicrofluidics*, 2010. **4**(2): p. 022811.
26. Castellarnau, M., et al., Dielectrophoresis as a Tool to Characterize and Differentiate Isogenic Mutants of Escherichia coli. *Biophysical journal*, 2006. **91**(10): p. 3937-3945.
27. P. Sabounchi, D. E. H., M. P. Kanouff, A. E. Harris, and B. A. Simmons, Joule Heating Effects on Insulator-Based Dielectrophoresis. *presented at the Twelfth International Conferences on Miniaturized Systems for Chemistry and Life Sciences, San Diego, CA, USA, ,* 2008.
28. Sabounchi, P., et al., Sample concentration and impedance detection on a microfluidic polymer chip. *Biomedical Microdevices*, 2008. **10**(5): p. 661-670.
29. Gantz, K., L. Renaghan, and M. Agah, Development of a comprehensive model for RIE-lag-based three-dimensional microchannel fabrication. *Journal of Micromechanics and Microengineering*, 2008. **18**(2): p. 025003.
30. Hosseini, Y., P. Zellner, and M. Agah, A Single-Mask Process for 3-D Microstructure Fabrication in PDMS. *Microelectromechanical Systems, Journal of*, 2013. **22**(2): p. 356-362.
31. Zellner, P., et al., A fabrication technology for three-dimensional micro total analysis systems. *Journal of Micromechanics and Microengineering*, 2010. **20**(4).
32. Shafiee, H., et al., Selective isolation of live/dead cells using contactless dielectrophoresis (cDEP). *Lab on a Chip*, 2010. **10**(4): p. 438-445.
33. Braff, W. A., A. Pignier, and C. R. Buie, High sensitivity three-dimensional insulator-based dielectrophoresis. *Lab on a Chip*, 2012. **12**(7): p. 1327-1331.
34. Markx, G. H., P. A. Dyda, and R. Pethig, Dielectrophoretic separation of bacteria using a conductivity gradient. *Journal of biotechnology*, 1996. **51**(2): p. 175-180.
35. Huang, Y., et al., Introducing dielectrophoresis as a new force field for field-flow fractionation. *Biophysical Journal*, 1997. **73**(2): p. 1118-1129.
36. Morgan, H., M. P. Hughes, and N. G. Green, Separation of Submicron Bioparticles by Dielectrophoresis. *Biophysical Journal*, 1999. **77**(1): p. 516-525.
37. Washizu, M., et al., Molecular dielectrophoresis of biopolymers. *Industry Applications, IEEE Transactions on*, 1994. **30**(4): p. 835-843.

38. Zellner, P., et al., 3D Insulator-based dielectrophoresis using DC-biased, AC electric fields for selective bacterial trapping. *ELECTROPHORESIS*, 2015. **36**(2): p. 277-283.
39. Zellner, P., et al., Off-chip passivated-electrode, insulator-based dielectrophoresis (OπDEP). *Analytical and bioanalytical chemistry*, 2013: p. 1-10.
40. Khoshmanesh, K., et al., Dielectrophoretic platforms for bio-microfluidic systems. *Biosensors and Bioelectronics*, 2011. **26**(5): p. 1800-1814.
41. Cui, H.-H., et al., Separation of particles by pulsed dielectrophoresis. *Lab on a Chip*, 2009. **9**(16): p. 2306-2312.
42. Kumemura, M., et al., Single-DNA-molecule trapping with silicon nanotweezers using pulsed dielectrophoresis. *Journal of Micromechanics and Microengineering*, 2011. **21**(5): p. 054020.

APPENDIX A: LIST OF PUBLICATIONS

1. Nakidde, Diana, Phillip Zellner, Mohammad Mehdi Alemi, Tyler Shake, Yahya Hosseini, Maria V. Riquelme, Amy Pruden, and Masoud Agah. "*Three dimensional passivated-electrode insulator-based dielectrophoresis*." Biomicrofluidics vol. 9, no. 1 (2015): 014125.
2. Phillip Zellner, Tyler Shake, Yahya Hosseini, Diana Nakidde, Maria V. Riquelme, Ali Sahari, Amy Pruden, Bahareh Behkam, and Masoud Agah, "*3D insulator-based dielectrophoresis using DC-biased, AC electric fields for selective bacterial trapping*," Electrophoresis, vol. 36, no. 2, January 2015, pp. 277-283.
3. V. Srinivasaraghavan, D. Aggarwal, H. Babahosseini, D. Nakidde, J. Strobl and M. Agah, "*Analyses of single-cell mechanoelectrical properties via microfluidics*," IEEE Sensors 2014, November 2014, Valencia, Spain.
4. Diana Nakidde, Phillip Zellner, Mohammad Mehdi Alemi and Masoud Agah, "*Three Dimensional Passivated-Electrode Insulator-Based Dielectrophoresis(3D πDEP)*," 18th International Conference on Miniaturized Systems for Chemistry and Life Sciences (MicroTAS 2014), October 2014, San Antonio, TX.
5. Diana Nakidde and Masoud Agah, "*Trapping of Submicron Beads using 3D Embedded-electrode Insulator-based Dielectrophoresis (3D-EπDEP)*," Biomedical Engineering Society (BMES) Annual Meeting 2014, October 2014, San Antonio, TX.
6. Kevin Crowley, Diana Nakidde, Jeff Travis, and Masoud Agah, "*Paper-based MEMS Hair Cell Array*," IEEE Sensors 2013, November 2013, Baltimore, MD, pp. 4.